

# Radiative corrections to Higgs-boson production in association with top-quark pairs at $e^+e^-$ colliders

A. DENNER<sup>1</sup>, S. DITTMAYER<sup>2</sup>, M. ROTH<sup>3</sup> AND M. M. WEBER<sup>1</sup>

<sup>1</sup> *Paul Scherrer Institut, Würenlingen und Villigen  
CH-5232 Villigen PSI, Switzerland*

<sup>2</sup> *Max-Planck-Institut für Physik (Werner-Heisenberg-Institut)  
D-80805 München, Germany*

<sup>3</sup> *Institut für Theoretische Physik, Universität Karlsruhe  
D-76128 Karlsruhe, Germany*

## Abstract:

We have calculated the complete  $\mathcal{O}(\alpha)$  and  $\mathcal{O}(\alpha_s)$  radiative corrections to the Higgs-production process  $e^+e^- \rightarrow t\bar{t}H$  in the Standard Model. This process is particularly interesting for the measurement of the top-quark Yukawa coupling at a future  $e^+e^-$  collider. The calculation of the  $\mathcal{O}(\alpha)$  corrections is described in some detail including, in particular, the treatment of the soft and collinear singularities. The discussion of numerical results focuses on the total cross section as well as on angular and energy distributions of the outgoing particles. The electroweak corrections turn out to be sizable and can reach the order of  $\pm 10\%$ . They result from cancellations between electromagnetic, fermionic, and weak bosonic corrections, each of which are of the order of  $\pm 10\%$ .

September 2003

# 1 Introduction

One of the main tasks at future colliders is the unraveling of the mechanism of electroweak symmetry breaking. In the Standard Model (SM) electroweak symmetry breaking is implemented via the Higgs–Kibble mechanism, which is responsible for the generation of particle masses and which leads to the prediction of a physical scalar particle, the Higgs boson. The mass of the Higgs boson is expected to be in the range between the current lower experimental bound of 114.4 GeV [ 1] and 1 TeV. Electroweak precision tests yield a 95% CL upper limit on the mass of the SM Higgs boson of 211 GeV [ 2]. A SM Higgs boson in the mass range up to 1 TeV will be discovered at the LHC, provided it exists and has no exotic properties. However, for the complete determination of its profile, including its couplings to fermions and gauge bosons, experiments in the clean environment of an  $e^+e^-$  linear collider [ 3] are indispensable.

The fermion masses in the SM are generated from the Yukawa interactions via a finite vacuum expectation value  $v = (\sqrt{2}G_\mu)^{-1/2} \approx 246$  GeV of the Higgs-boson field. The strength of the coupling of the physical Higgs boson to fermions is fixed by  $g_{f\bar{f}H} = m_f/v$  in lowest order. The measurement of these Yukawa couplings is therefore important in order to verify the mass-generation mechanism of the SM. By far the largest Yukawa coupling is the top-quark–Higgs-boson coupling ( $g_{t\bar{t}H}^2 \approx 0.5$ ) owing to the large top-quark mass. Its measurement is therefore especially interesting.

A direct access to the top-quark Yukawa coupling is provided by the process  $e^+e^- \rightarrow t\bar{t}H$  [ 4] if the Higgs-boson mass is not too large, i.e.  $M_H \sim 100\text{--}200$  GeV. This process proceeds mainly through Higgs-boson emission off top quarks, while emission from intermediate Z bosons plays only a minor role, making it suitable for a determination of  $g_{t\bar{t}H}$ . If the Higgs boson is light, i.e.  $M_H \sim 120$  GeV, a precision of around 5% can be reached at an  $e^+e^-$  linear collider operating at  $\sqrt{s} = 800$  GeV with a luminosity of  $\int L dt \sim 1000 \text{ fb}^{-1}$  [ 5]. Combining the  $t\bar{t}H$  channel with information from other Higgs-production and decay processes an even better accuracy can be obtained in a combined fit [ 6]. Furthermore, by investigating the process  $e^+e^- \rightarrow t\bar{t}H$  bounds on non-standard physics in the top-quark Yukawa coupling can be derived [ 4, 7].

Assuming an experimental precision of a few per cent, a thorough understanding of the background to the  $t\bar{t}H$  final state is necessary [ 8], and precise theoretical predictions for the signal process  $e^+e^- \rightarrow t\bar{t}H$  at the per-cent level are needed. This requires the inclusion of radiative corrections, a rather complicated task for a process with three massive unstable particles in the final state. As a first step, the process  $e^+e^- \rightarrow t\bar{t}H$  can be treated in the approximation of stable top quarks and Higgs bosons. The corresponding leading-order total cross section is already known for a long time [ 9]. The  $\mathcal{O}(\alpha_s)$  corrections to the total cross section within the SM have been calculated first in the “effective Higgs-boson approximation” valid only for small Higgs-boson masses and very high energies [ 10]. A calculation of all diagrams for the dominant photon-exchange channel has been performed in Ref. [ 11], while the full set of diagrams has been evaluated in Ref. [ 12]. Within the Minimal Supersymmetric Standard Model (MSSM) the  $\mathcal{O}(\alpha_s)$  corrections to the production cross sections of neutral Higgs bosons in association with heavy quark pairs ( $t\bar{t}$ ,  $b\bar{b}$ ) have been calculated in Ref. [ 13] for the photon-exchange channel. In Ref. [ 14] all QCD diagrams have been taken into account, while the SUSY-QCD corrections have

been worked out in Ref. [15]. Furthermore, the  $\mathcal{O}(\alpha_s)$  corrections to the Higgs-boson energy distribution both in the SM and the MSSM have been discussed in Ref. [16].

Recently, considerable progress has been achieved in the calculation of the electroweak corrections to  $e^+e^- \rightarrow t\bar{t}H$ . Results for the electroweak  $\mathcal{O}(\alpha)$  corrections in the SM have been presented in Refs. [17, 18]. A calculation of some top-mass enhanced electroweak corrections in the SM, the MSSM, and the two-Higgs doublet model has been performed in Ref. [19].

We have accomplished a completely independent calculation of the  $\mathcal{O}(\alpha)$  electroweak corrections to the process  $e^+e^- \rightarrow t\bar{t}H$  in the SM as well as of the  $\mathcal{O}(\alpha_s)$  QCD corrections. First results for total cross sections have already been presented in Ref. [20] including a comparison of our results with those of Refs. [17, 18]. While we find good agreement with Ref. [18], our results differ from those of Ref. [17] at high centre-of-mass (CM) energies and close to threshold. Moreover, we reproduced the results of Ref. [12] for the QCD corrections to this process.

In this paper we present details of our calculation. Single hard-photon radiation is included using the complete matrix element and combined with the virtual corrections applying both phase-space-slicing and subtraction methods. Higher-order corrections from initial-state photon radiation (ISR) are taken into account in the leading-logarithmic approximation. Moreover, we supplement our previous work with results for distributions in the energies and production angles of the Higgs boson and the top quark. Results on electroweak corrections to differential cross sections have not yet been presented in the literature before.

The paper is organized as follows: in Section 2 the calculation of the virtual and real corrections is described. Section 3 contains a discussion of numerical results. The paper is summarized in Section 4. Further useful information on the calculation of the matrix elements is collected in the appendices.

## 2 Calculation of radiative corrections

### 2.1 Conventions and lowest-order cross section

We consider the process

$$e^-(p_1, \sigma_1) + e^+(p_2, \sigma_2) \longrightarrow t(k_1, \tau_1) + \bar{t}(k_2, \tau_2) + H(k_3), \quad (2.1)$$

where the momenta  $p_a$ ,  $k_i$  of the particles and the helicities of the electrons,  $\sigma_a$ , and top quarks,  $\tau_i$ , are given in parentheses. The helicities take the values  $\sigma_a, \tau_i = \pm 1/2$ , but we often use only the sign to indicate the helicity. The electron mass is neglected whenever possible, i.e. it is kept finite only in the mass-singular logarithms related to ISR. This implies that the lowest-order and one-loop amplitudes vanish unless  $\sigma_1 = -\sigma_2$ . Therefore, we define  $\sigma = \sigma_1 = -\sigma_2$ . The particle momenta obey the mass-shell conditions  $p_1^2 = p_2^2 = 0$ ,  $k_1^2 = k_2^2 = m_t^2$ , and  $k_3^2 = M_H^2$ . For later use, the following set of kinematical invariants is defined:

$$\begin{aligned} s &= (p_1 + p_2)^2, \\ s_{ij} &= (k_i + k_j)^2, & i, j &= 1, 2, 3, \\ t_{ai} &= (p_a - k_i)^2, & a &= 1, 2, & i &= 1, 2, 3. \end{aligned} \quad (2.2)$$

Using the conventions of Ref. [ 21] we generically denote the couplings of the neutral bosons to the fermions in the following by

$$\begin{aligned}
g_{\gamma f}^{\pm} &= -Q_f, & g_{Zf}^+ &= -\frac{s_w}{c_w}Q_f, & g_{Zf}^- &= -\frac{s_w}{c_w}Q_f + \frac{I_{w,f}^3}{c_w s_w}, \\
g_{Hf}^{\pm} &= g_{Hf} = -\frac{1}{2s_w}\frac{m_f}{M_W}, & g_{\chi f}^{\pm} &= \pm g_{\chi f} = \pm \frac{iI_{w,f}^3}{s_w}\frac{m_f}{M_W}, \\
g_{ZZH} &= \frac{M_Z}{s_w c_w}, & g_{Z\chi H} &= \frac{-i}{2s_w c_w},
\end{aligned} \tag{2.3}$$

where  $Q_f$  is the relative charge of the fermion  $f$ , and  $I_{w,f}^3 = \pm 1/2$  the third component of the weak isospin of the left-handed part of the fermion field  $f$ . The sine and cosine of the weak mixing angle are fixed by

$$c_w^2 = 1 - s_w^2 = \frac{M_W^2}{M_Z^2}. \tag{2.4}$$

In order to express the amplitude for the bremsstrahlung process  $e^+e^- \rightarrow t\bar{t}H\gamma$  in a compact way (see Section 2.3.1), we use the Weyl–van der Waerden spinor technique as formulated in Ref. [ 22]. The helicity states for the massless electrons and massive top quarks are constructed as follows. Those for the massless incoming electron with momentum

$$p_1^\mu = p_1^0(1, \cos \phi_{p_1} \sin \theta_{p_1}, \sin \phi_{p_1} \sin \theta_{p_1}, \cos \theta_{p_1}) \tag{2.5}$$

can be constructed from the Weyl spinor

$$p_{1,A} = \sqrt{2p_1^0} \begin{pmatrix} e^{-i\phi_{p_1}} \cos \frac{\theta_{p_1}}{2} \\ \sin \frac{\theta_{p_1}}{2} \end{pmatrix}, \tag{2.6}$$

and the corresponding momentum matrix reads

$$P_{1,\dot{A}B} = p_{1,\dot{A}} p_{1,B}. \tag{2.7}$$

The spinor  $p_{2,A}$  and the momentum matrix  $P_{2,\dot{A}B}$  of the incoming positron are defined analogously.

The spinors  $\rho_{i,A}$  corresponding to the top-quark momentum

$$k_1^\mu = (k_1^0, |\mathbf{k}_1| \cos \phi_{k_1} \sin \theta_{k_1}, |\mathbf{k}_1| \sin \phi_{k_1} \sin \theta_{k_1}, |\mathbf{k}_1| \cos \theta_{k_1}) \tag{2.8}$$

are defined as

$$\rho_{1,A} = \sqrt{k_1^0 + |\mathbf{k}_1|} \begin{pmatrix} e^{-i\phi_{k_1}} \cos \frac{\theta_{k_1}}{2} \\ \sin \frac{\theta_{k_1}}{2} \end{pmatrix}, \quad \rho_{2,A} = \sqrt{k_1^0 - |\mathbf{k}_1|} \begin{pmatrix} \sin \frac{\theta_{k_1}}{2} \\ -e^{+i\phi_{k_1}} \cos \frac{\theta_{k_1}}{2} \end{pmatrix}. \tag{2.9}$$

They obey the relation

$$\langle \rho_2 \rho_1 \rangle = m_t, \tag{2.10}$$

where the spinor product is defined by

$$\langle \phi \psi \rangle = \phi_A \epsilon^{AB} \phi_B = \phi_1 \psi_2 - \phi_2 \psi_1. \tag{2.11}$$

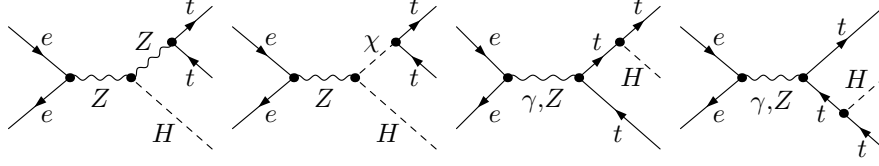


Figure 1: Tree-level diagrams for  $e^+e^- \rightarrow t\bar{t}H$

The spinors  $\rho'_{i,A}$  corresponding to  $k_2$  are constructed in the same way. The momentum matrices  $K_1$  and  $K_2$  corresponding to the outgoing momenta  $k_1$  and  $k_2$  are decomposed into the spinors  $\rho_{i,A}$  and  $\rho'_{i,A}$ , respectively,

$$K_{1,\dot{A}B} = \sum_{i=1,2} \rho_{i,\dot{A}} \rho_{i,B}, \quad K_{2,\dot{A}B} = \sum_{i=1,2} \rho'_{i,\dot{A}} \rho'_{i,B}. \quad (2.12)$$

The Dirac spinors of the outgoing (anti-)top quarks are generically given by

$$\bar{u}_t(k_1) = (\eta^A, \xi_{\dot{A}}), \quad v_{\bar{t}}(k_2) = \begin{pmatrix} \xi'_{\dot{A}} \\ \eta'^A \end{pmatrix} \quad (2.13)$$

with the actual insertions

$$(\xi, \eta) = \begin{cases} (\rho_1, -\rho_2) & \text{for } \tau_1 = +, \\ (\rho_2, \rho_1) & \text{for } \tau_1 = -, \end{cases} \quad (\xi', \eta') = \begin{cases} (\rho'_1, \rho'_2) & \text{for } \tau_2 = -, \\ (-\rho'_2, \rho'_1) & \text{for } \tau_2 = +, \end{cases} \quad (2.14)$$

i.e. we have  $\langle \xi \eta \rangle = \langle \eta' \xi' \rangle = m_t$ .

Although the Higgs boson has spin 0, it is convenient to express its momentum in terms of Weyl spinors  $\phi_{i,A}$ . These are obtained from the momentum  $k_3$  analogously to (2.9). Then the momentum matrix  $K_3$  of the Higgs boson can be decomposed as

$$K_{3,\dot{A}B} = \sum_{i=1,2} \phi_{i,\dot{A}} \phi_{i,B}. \quad (2.15)$$

It is instructive to give the lowest-order amplitude for  $e^+e^- \rightarrow t\bar{t}H$  in this formalism. It receives contributions of the four diagrams shown in Figure 1:

$$\mathcal{M}_0^{\sigma\tau_1\tau_2} = \mathcal{M}_0^{Z,\sigma\tau_1\tau_2} + \mathcal{M}_0^{\chi,\sigma\tau_1\tau_2} + \sum_{V=\gamma,Z} \left( \mathcal{M}_0^{Vt,\sigma\tau_1\tau_2} + \mathcal{M}_0^{V\bar{t},\sigma\tau_1\tau_2} \right), \quad (2.16)$$

where the upper indices  $Z, \chi, t, \bar{t}$  indicate the particle from which the Higgs boson is emitted. In the 't Hooft–Feynman gauge, the contributions corresponding to these four diagrams read

$$\begin{aligned} \mathcal{M}_0^{Z,\sigma\tau_1\tau_2} &= 2 e^3 g_{Ze}^\sigma g_{ZZH} P_Z(p_1 + p_2) P_Z(k_1 + k_2) A_{\sigma\tau_1\tau_2}^Z(p_1, p_2, k_1, k_2), \\ \mathcal{M}_0^{\chi,\sigma\tau_1\tau_2} &= -2 e^3 g_{Ze}^\sigma g_{Z\chi H} g_{\chi t} P_Z(p_1 + p_2) P_Z(k_1 + k_2) A_{\sigma\tau_1\tau_2}^\chi(p_1, p_2, k_1, k_2), \\ \mathcal{M}_0^{Vt,\sigma\tau_1\tau_2} &= -2 e^3 g_{Ve}^\sigma g_{Ht} P_V(p_1 + p_2) P_t(k_1 + k_3) A_{\sigma\tau_1\tau_2}^{Vt}(p_1, p_2, k_1, k_2), \\ \mathcal{M}_0^{V\bar{t},\sigma\tau_1\tau_2} &= -2 e^3 g_{Ve}^\sigma g_{H\bar{t}} P_V(p_1 + p_2) P_{\bar{t}}(k_2 + k_3) A_{\sigma\tau_1\tau_2}^{V\bar{t}}(p_1, p_2, k_1, k_2) \end{aligned} \quad (2.17)$$

with the auxiliary functions

$$\begin{aligned}
A_{+,\tau_1,\tau_2}^Z(p_1, p_2, k_1, k_2) &= g_{Zt}^+ \langle p_2 \xi \rangle^* \langle p_1 \xi' \rangle + g_{Zt}^- \langle p_2 \eta' \rangle^* \langle p_1 \eta \rangle, \\
A_{+,\tau_1,\tau_2}^X(p_1, p_2, k_1, k_2) &= (\langle \xi' \eta \rangle - \langle \xi \eta' \rangle^*) \langle p_2 K_3 p_1 \rangle, \\
A_{+,\tau_1,\tau_2}^{Vt}(p_1, p_2, k_1, k_2) &= g_{Vt}^- \langle p_2 \eta' \rangle^* (2m_t \langle p_1 \eta \rangle + \langle \xi K_3 p_1 \rangle) \\
&\quad + g_{Vt}^+ \langle p_1 \xi' \rangle (2m_t \langle p_2 \xi \rangle^* - \langle p_2 K_3 \eta \rangle), \\
A_{+,\tau_1,\tau_2}^{V\bar{t}}(p_1, p_2, k_1, k_2) &= g_{Vt}^+ \langle p_2 \xi \rangle^* (2m_t \langle p_1 \xi' \rangle + \langle \eta' K_3 p_1 \rangle) \\
&\quad + g_{Vt}^- \langle p_1 \eta \rangle (2m_t \langle p_2 \eta' \rangle^* - \langle p_2 K_3 \xi' \rangle), \\
A_{-\sigma,\tau_1,\tau_2}^{\dots}(p_1, p_2, k_1, k_2) &= A_{\sigma\tau_1\tau_2}^{\dots}(p_2, p_1, k_1, k_2).
\end{aligned} \tag{2.18}$$

Here we used the shorthand notation

$$\langle \psi' K_3 \psi \rangle = \psi'_A K_3^{AB} \psi_B = \sum_{i=1,2} \langle \psi' \phi_i \rangle^* \langle \psi \phi_i \rangle \tag{2.19}$$

and abbreviated the propagators as

$$P_t(p) = \frac{1}{p^2 - m_t^2}, \quad P_Z(p) = \frac{1}{p^2 - M_Z^2}, \quad P_\gamma(p) = \frac{1}{p^2}. \tag{2.20}$$

Note that there is no need to introduce a finite width since none of the internal lines can become resonant for the physical top-quark and Higgs-boson masses. Finally, the lowest-order cross section reads

$$\sigma_0 = \frac{1}{2s} \int d\Phi_3 \sum_{\sigma=\pm\frac{1}{2}} \frac{1}{4} (1 + 2P_- \sigma)(1 - 2P_+ \sigma) |\mathcal{M}_0^\sigma|^2, \tag{2.21}$$

where

$$|\mathcal{M}_0^\sigma|^2 = N_t^c \sum_{\tau_1=\pm\frac{1}{2}} \sum_{\tau_2=\pm\frac{1}{2}} |\mathcal{M}_0^{\sigma\tau_1\tau_2}|^2 \tag{2.22}$$

with the colour factor  $N_t^c = 3$  of the top quark,  $P_\pm$  are the degrees of polarization of the  $e^\pm$  beams, and the integral over the three-particle phase space is defined by

$$\int d\Phi_3 = \left( \prod_{i=1}^3 \int \frac{d^3 \mathbf{k}_i}{(2\pi)^3 2k_i^0} \right) (2\pi)^4 \delta \left( p_1 + p_2 - \sum_{j=1}^3 k_j \right). \tag{2.23}$$

## 2.2 Virtual corrections

### 2.2.1 Survey of one-loop diagrams

The virtual corrections receive contributions from self-energy, vertex, box, and pentagon diagrams. The structural diagrams containing the generic contributions of vertex functions are summarized in Figure 2. The full set of pentagon diagrams is shown in Figure 3.

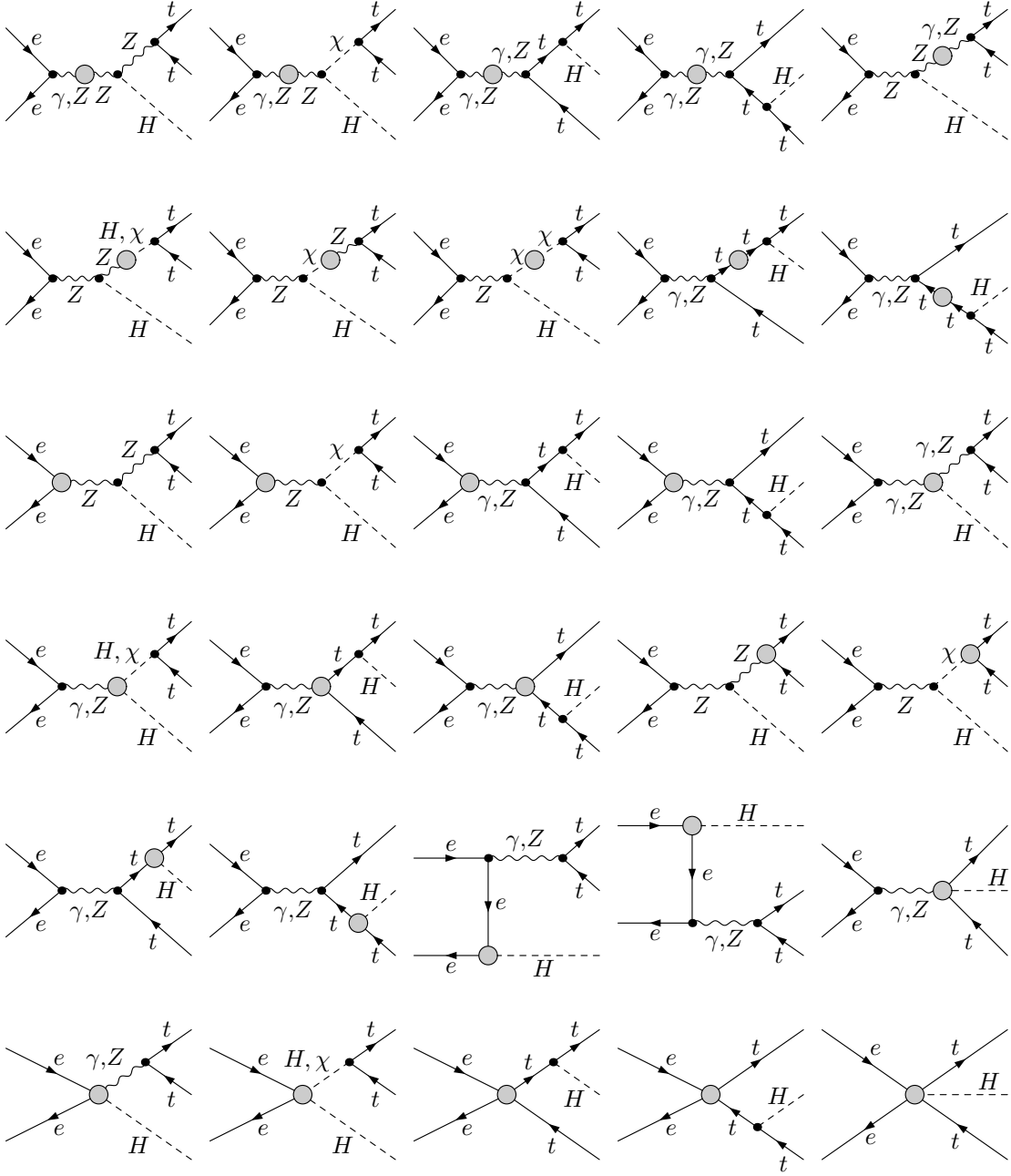


Figure 2: Contributions of different vertex functions to  $e^+e^- \rightarrow t\bar{t}H$

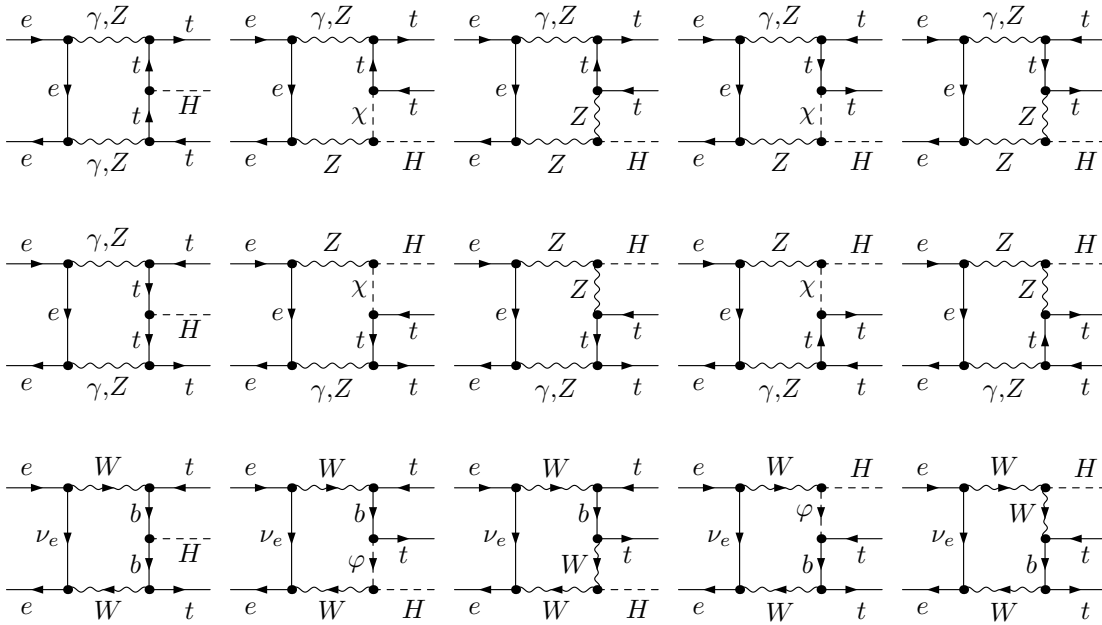


Figure 3: Pentagon diagrams for  $e^+e^- \rightarrow t\bar{t}H$

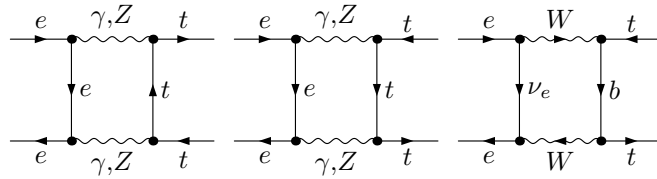


Figure 4:  $e^+e^-t\bar{t}$  box diagrams

The box diagrams for the  $e^+e^-t\bar{t}$  vertex function are shown in Figure 4, the  $e^+e^-HH$  box diagrams in Figure 5, and the  $e^+e^-H\chi$  box diagrams in Figure 6. Figure 7 lists the diagrams for the  $\gamma t\bar{t}H$  and  $Zt\bar{t}H$  vertex functions. In Figure 7, as well as in Figure 10, diagrams that can be obtained by reversing the charge flow of all charged particles are not shown. The  $e^+e^-ZH$  box diagrams can be found in Ref. [23], and the  $e^+e^-\gamma H$  diagrams can be obtained from a subset of those.

The diagrams contributing to the  $\gamma t\bar{t}$  and  $Zt\bar{t}$  vertex functions are depicted in Figure 8, the  $Ht\bar{t}$  and  $\chi t\bar{t}$  diagrams in Figure 9, and Figure 10 shows the  $\gamma H\chi$  and  $ZH\chi$  diagrams. The diagrams for the  $\gamma ZH$ ,  $ZZH$ , and  $e^+e^-H$  vertex functions are shown in Ref. [23]. Those for the  $\gamma\gamma H$  vertex function can be obtained from a subset of the  $\gamma ZH$  vertex diagrams. The  $e^+e^-\gamma$  and  $e^+e^-Z$  diagrams and most of the self-energy diagrams can be found in Ref. [24]. The diagrams for the top-quark self-energy are listed in Figure 11. The  $ZH$ -mixing energy and the  $\gamma HH$  and  $ZHH$  vertex functions vanish owing to CP symmetry.

All pentagon and box diagrams are ultraviolet (UV) finite, as well as the  $\gamma\gamma H$  vertex function. Since we neglect the electron mass whenever possible, also the  $e^+e^-H$  vertex function is UV finite. The remaining vertex functions and self-energies are UV divergent, and the corresponding counterterm diagrams have to be included.

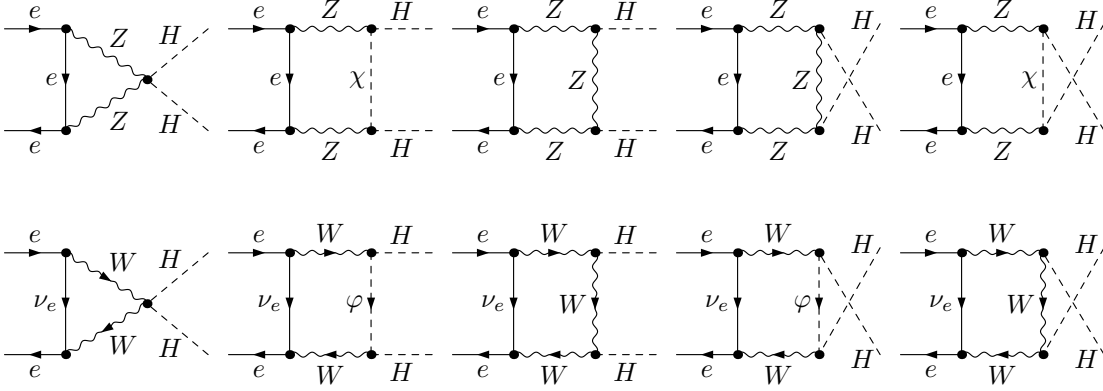


Figure 5:  $e^+e^-HH$  box diagrams

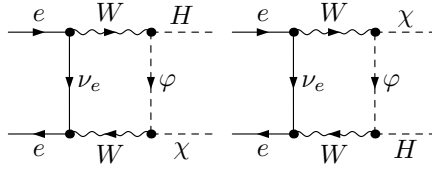


Figure 6:  $e^+e^-H\chi$  box diagrams

### 2.2.2 Computational framework

The actual calculation of the one-loop diagrams closely follows the strategy of Ref. [23], where the  $\mathcal{O}(\alpha)$  corrections to  $e^+e^- \rightarrow \nu\bar{\nu}H$  have been calculated, i.e. it has been carried out in the 't Hooft–Feynman gauge using standard techniques. The Feynman graphs have been generated with *FeynArts* [25] and are evaluated in two completely independent ways, leading to two independent computer codes. The results of the two codes are in good numerical agreement (i.e. within about 12 digits for non-exceptional phase-space points). Apart from the 5-point integrals, the tensor coefficients of the one-loop integrals are algebraically reduced to scalar integrals with the Passarino–Veltman algorithm [26] at the numerical level. For the evaluation of the tensor 5-point functions the direct reduction to 4-point integrals of Ref. [27] has been used. This method avoids leading inverse Gram determinants which cause numerical instabilities at the phase-space boundaries. The scalar integrals are evaluated using the methods and results of Refs. [21, 28], where UV divergences are regulated dimensionally and infrared (IR) divergences with an infinitesimal photon mass  $m_\gamma$ . The soft and collinear singularities of some scalar 5-point integrals have been checked against the general result of Ref. [29]. The renormalization is carried out in the on-shell renormalization scheme, as e.g. described in Ref. [21].

In the first calculation, the Feynman graphs are generated with *FeynArts* version 1.0 [25]. With the help of *Mathematica* routines the amplitudes are expressed in terms of standard matrix elements (SME) and coefficients of tensor integrals, as described in the appendices in more detail. The output is processed into a *Fortran* program for the numerical evaluation. The second calculation has been made using *FeynArts* version 3

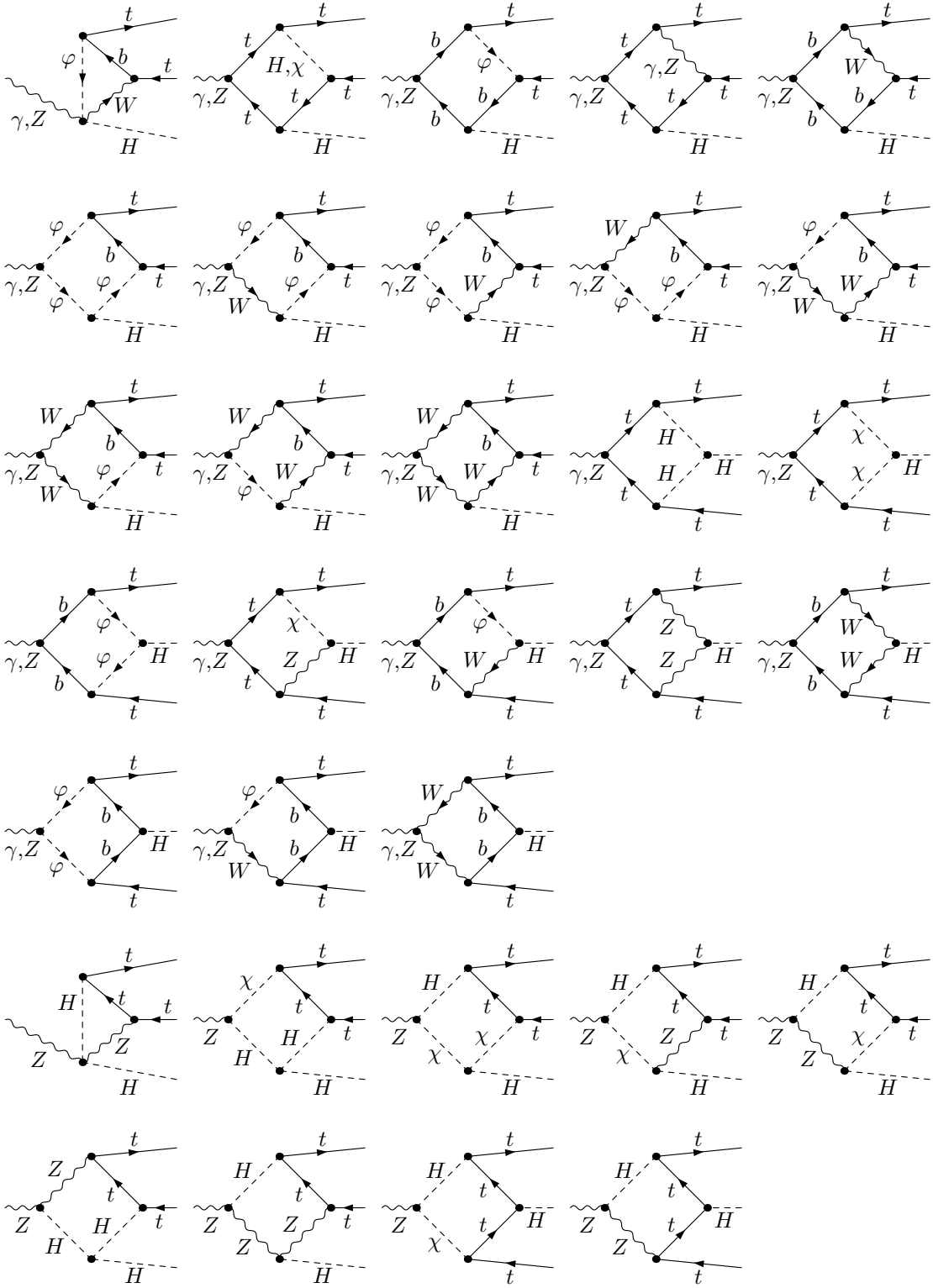


Figure 7:  $\gamma t\bar{t}H$  and  $Zt\bar{t}H$  box diagrams (Diagrams with reversed charge flow are not shown.)

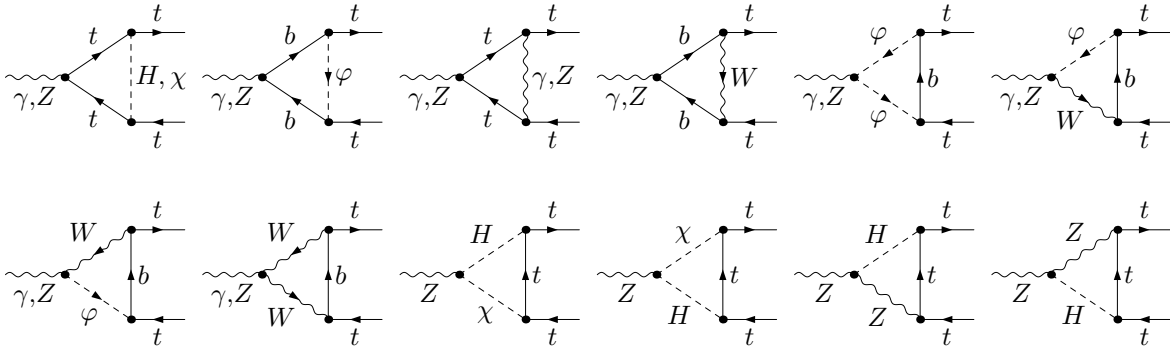


Figure 8: Diagrams for  $\gamma t\bar{t}$  and  $Z t\bar{t}$  vertex functions

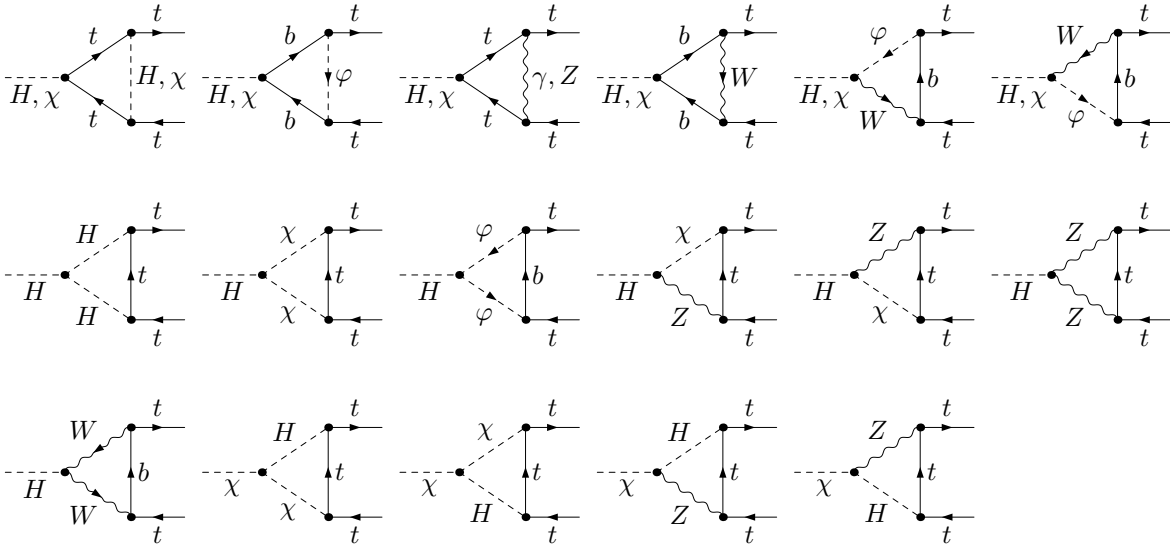


Figure 9: Diagrams for  $H t\bar{t}$  and  $\chi t\bar{t}$  vertex functions

[ 30] for the generation and *FormCalc* [ 31] for the evaluation of the amplitudes. The analytical results of *FormCalc* in terms of SME and their coefficients were translated into *C++* code for numerical evaluation.

As a check of gauge invariance the calculation of the virtual corrections has been repeated using the background-field method [ 32], where the individual contributions from self-energy, vertex, box, and pentagon corrections differ from their counterparts in the conventional formalism. The total one-loop corrections of the conventional and of the background-field approach were found to be in perfect numerical agreement.

Finally, the contribution of the virtual corrections to the cross section is given by

$$\delta\sigma_{\text{virt}} = \frac{1}{2s} \int d\Phi_3 \sum_{\sigma=\pm\frac{1}{2}} \frac{1}{4} (1 + 2P_{-\sigma})(1 - 2P_{+\sigma}) N_t^c \sum_{\tau_1=\pm\frac{1}{2}} \sum_{\tau_2=\pm\frac{1}{2}} 2 \text{Re} \{ \mathcal{M}_1^{\sigma\tau_1\tau_2} (\mathcal{M}_0^{\sigma\tau_1\tau_2})^* \}, \quad (2.24)$$

where  $\mathcal{M}_1^{\sigma\tau_1\tau_2}$  denotes the one-loop helicity amplitudes.

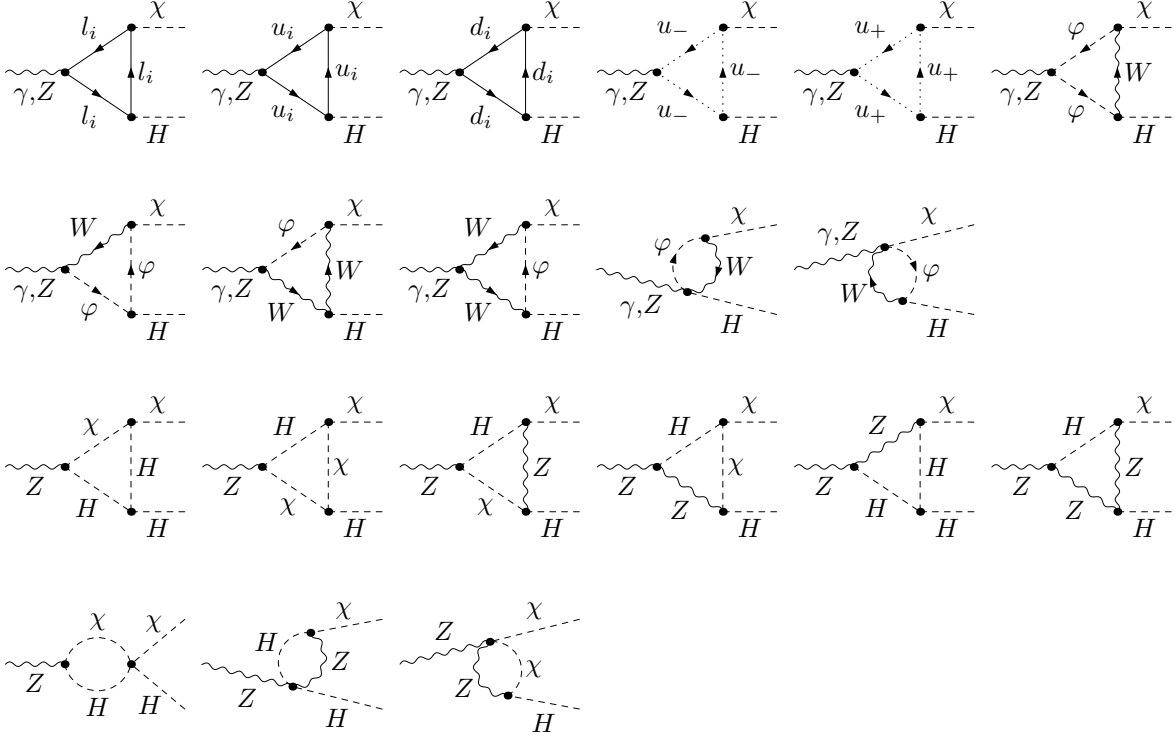


Figure 10: Diagrams for  $\gamma H\chi$  and  $ZH\chi$  vertex functions (Diagrams with reversed charge flow in the loop are not shown.)

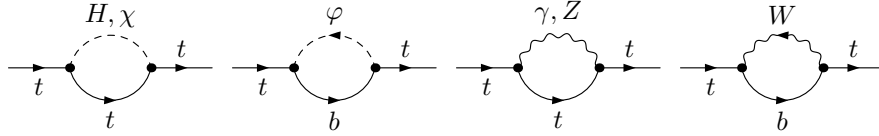


Figure 11: Diagrams contributing to the top-quark self-energy

## 2.3 Real photonic corrections

### 2.3.1 Matrix-element calculation

The real photonic corrections are induced by the process

$$e^-(p_1, \sigma_1) + e^+(p_2, \sigma_2) \longrightarrow t(k_1, \tau_1) + \bar{t}(k_2, \tau_2) + H(k_3) + \gamma(k, \lambda), \quad (2.25)$$

where  $k$  and  $\lambda$  denote the photon momentum and helicity, respectively. The Feynman diagrams of this process are shown in Figure 12. We have evaluated the corresponding helicity matrix elements  $\mathcal{M}_\gamma^{\sigma\tau_1\tau_2\lambda}$  using the Weyl–van der Waerden spinor technique as formulated in Ref. [22]. The amplitudes for the helicity channels with  $\sigma_1 = \sigma_2$  vanish for massless electrons, and we define  $\sigma = \sigma_1 = -\sigma_2$  as above. The treatment of IR (soft and collinear) singularities, where the finite electron mass is needed, is described below.

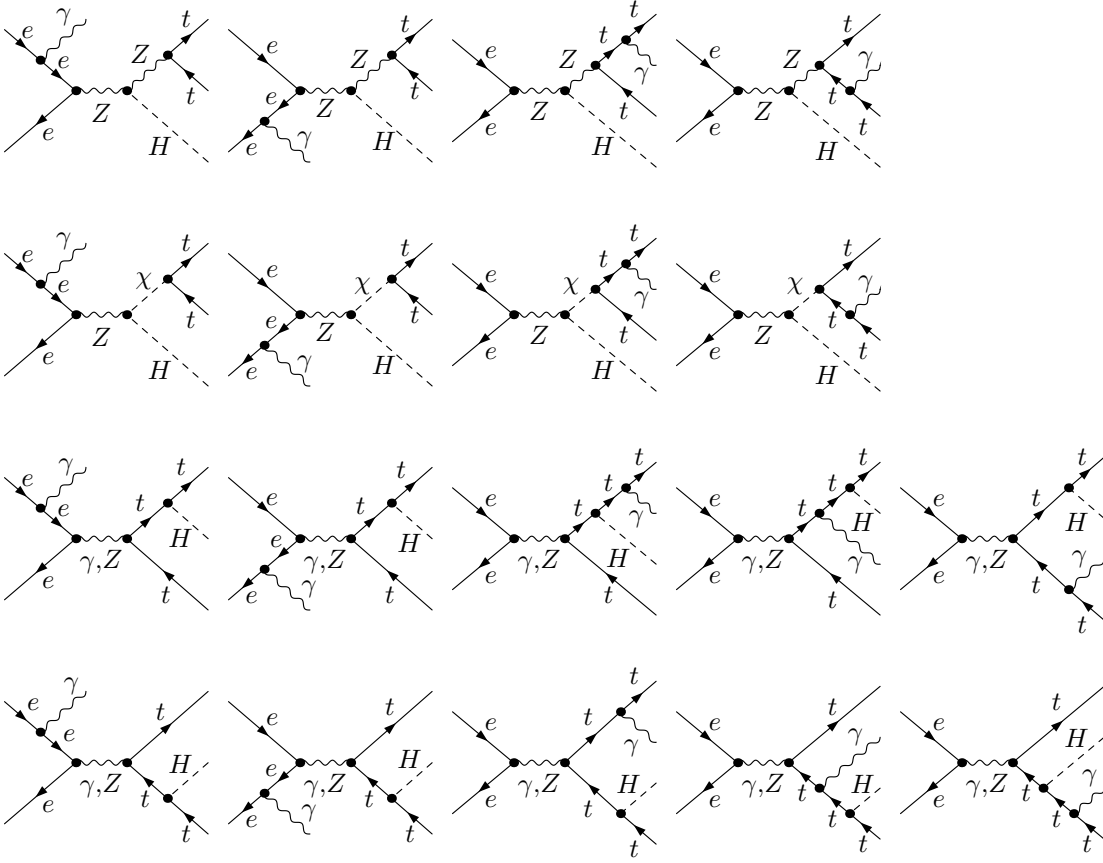


Figure 12: Feynman diagrams for  $e^+e^- \rightarrow t\bar{t}H\gamma$

The amplitude for  $e^+e^- \rightarrow t\bar{t}H\gamma$  can be separated into 12 contributions that are invariant with respect to gauge transformations of the external photon,

$$\begin{aligned} \mathcal{M}_\gamma^{\sigma\tau_1\tau_2\lambda} &= \mathcal{M}_\gamma^{Ze,\sigma\tau_1\tau_2\lambda} + \mathcal{M}_\gamma^{Zt,\sigma\tau_1\tau_2\lambda} + \mathcal{M}_\gamma^{\chi e,\sigma\tau_1\tau_2\lambda} + \mathcal{M}_\gamma^{\chi t,\sigma\tau_1\tau_2\lambda} \\ &+ \sum_{V=\gamma,Z} \left( \mathcal{M}_\gamma^{Vte,\sigma\tau_1\tau_2\lambda} + \mathcal{M}_\gamma^{Vtt,\sigma\tau_1\tau_2\lambda} + \mathcal{M}_\gamma^{V\bar{t}e,\sigma\tau_1\tau_2\lambda} + \mathcal{M}_\gamma^{V\bar{t}t,\sigma\tau_1\tau_2\lambda} \right). \end{aligned} \quad (2.26)$$

The last upper particle index in  $\mathcal{M}_\gamma^{Ze}$ , etc., indicates to which charged fermion line (e or t) the photon is attached. The diagrams in the first line of Figure 12 belong to  $\mathcal{M}_\gamma^{Ze}$  and  $\mathcal{M}_\gamma^{Zt}$ , those in the second line to  $\mathcal{M}_\gamma^{\chi e}$  and  $\mathcal{M}_\gamma^{\chi t}$ , those in the third line to  $\mathcal{M}_\gamma^{Vte}$  and  $\mathcal{M}_\gamma^{Vtt}$ , and those in the last line to  $\mathcal{M}_\gamma^{V\bar{t}e}$  and  $\mathcal{M}_\gamma^{V\bar{t}t}$ .

In the 't Hooft–Feynman gauge, the individual contributions read

$$\begin{aligned} \mathcal{M}_\gamma^{Ze,\sigma\tau_1\tau_2\lambda} &= 2\sqrt{2} e^4 g_{Ze}^\sigma g_{ZZH} P_Z(p_1 + p_2 - k) P_Z(k_1 + k_2) \\ &\times A_{\sigma\tau_1\tau_2\lambda}^{Ze}(p_1, p_2, k_1, k_2, k), \end{aligned} \quad (2.27)$$

$$\begin{aligned} \mathcal{M}_\gamma^{Zt,\sigma\tau_1\tau_2\lambda} &= -\sqrt{2} e^4 Q_t g_{Ze}^\sigma g_{ZZH} P_Z(p_1 + p_2) P_Z(k_1 + k_2 + k) \\ &\times A_{\sigma\tau_1\tau_2\lambda}^{Zt}(p_1, p_2, k_1, k_2, k), \end{aligned} \quad (2.28)$$

$$\begin{aligned}\mathcal{M}_\gamma^{\chi e, \sigma \tau_1 \tau_2 \lambda} &= 2\sqrt{2} e^4 g_{Z_e}^\sigma g_{Z_{\chi H}} g_{\chi t} P_Z(p_1 + p_2 - k) P_Z(k_1 + k_2) \\ &\quad \times A_{\sigma \tau_1 \tau_2 \lambda}^{\chi e}(p_1, p_2, k_1, k_2, k),\end{aligned}\quad (2.29)$$

$$\begin{aligned}\mathcal{M}_\gamma^{\chi t, \sigma \tau_1 \tau_2 \lambda} &= -2\sqrt{2} e^4 Q_t g_{Z_e}^\sigma g_{Z_{\chi H}} g_{\chi t} P_Z(p_1 + p_2) P_Z(k_1 + k_2 + k) \\ &\quad \times A_{\sigma \tau_1 \tau_2 \lambda}^{\chi t}(p_1, p_2, k_1, k_2, k),\end{aligned}\quad (2.30)$$

$$\begin{aligned}\mathcal{M}_\gamma^{V_{te}, \sigma \tau_1 \tau_2 \lambda} &= 2\sqrt{2} e^4 g_{V_e}^\sigma g_{Ht} P_V(p_1 + p_2 - k) P_t(k_1 + k_3) \\ &\quad \times A_{\sigma \tau_1 \tau_2 \lambda}^{V_{te}}(p_1, p_2, k_1, k_2, k),\end{aligned}\quad (2.31)$$

$$\mathcal{M}_\gamma^{V_{tt}, \sigma \tau_1 \tau_2 \lambda} = -2\sqrt{2} e^4 Q_t g_{V_e}^\sigma g_{Ht} P_V(p_1 + p_2) A_{\sigma \tau_1 \tau_2 \lambda}^{V_{tt}}(p_1, p_2, k_1, k_2, k), \quad (2.32)$$

$$\begin{aligned}\mathcal{M}_\gamma^{V_{\bar{t}e}, \sigma \tau_1 \tau_2 \lambda} &= 2\sqrt{2} e^4 g_{V_e}^\sigma g_{Ht} P_V(p_1 + p_2 - k) P_t(k_2 + k_3) \\ &\quad \times A_{\sigma \tau_1 \tau_2 \lambda}^{V_{\bar{t}e}}(p_1, p_2, k_1, k_2, k),\end{aligned}\quad (2.33)$$

$$\mathcal{M}_\gamma^{V_{\bar{t}t}, \sigma \tau_1 \tau_2 \lambda} = -2\sqrt{2} e^4 Q_t g_{V_e}^\sigma g_{Ht} P_V(p_1 + p_2) A_{\sigma \tau_1 \tau_2 \lambda}^{V_{\bar{t}t}}(p_1, p_2, k_1, k_2, k) \quad (2.34)$$

with the auxiliary functions

$$A_{+, \tau_1, \tau_2, +}^{Ze}(p_1, p_2, k_1, k_2, k) = -g_{Zt}^+ \langle p_1 \xi' \rangle \frac{\langle \xi (P_2 - K) p_1 \rangle}{\langle k p_1 \rangle \langle k p_2 \rangle} - g_{Zt}^- \langle p_1 \eta \rangle \frac{\langle \eta' (P_2 - K) p_1 \rangle}{\langle k p_1 \rangle \langle k p_2 \rangle},$$

$$\begin{aligned}A_{+, \tau_1, \tau_2, +}^{Zt}(p_1, p_2, k_1, k_2, k) &= \left( g_{Zt}^+ \langle p_2 \xi \rangle^* \langle p_1 \xi' \rangle + g_{Zt}^- \langle p_2 \eta' \rangle^* \langle p_1 \eta \rangle \right) \frac{\langle k K_2 K_1 k \rangle}{2(k_1 \cdot k)(k_2 \cdot k)} \\ &\quad + \langle k p_2 \rangle^* \left( \frac{g_{Zt}^+ \langle k \xi \rangle^*}{(k_1 \cdot k)} \langle p_1 \xi' \rangle - \frac{g_{Zt}^- \langle k \eta' \rangle^*}{(k_2 \cdot k)} \langle p_1 \eta \rangle \right),\end{aligned}$$

$$A_{+, \tau_1, \tau_2, +}^{\chi e}(p_1, p_2, k_1, k_2, k) = \left( \langle \xi \eta' \rangle^* - \langle \xi' \eta \rangle \right) \frac{\langle p_1 (P_2 - K) K_3 p_1 \rangle^*}{\langle k p_1 \rangle \langle k p_2 \rangle},$$

$$\begin{aligned}A_{+, \tau_1, \tau_2, +}^{\chi t}(p_1, p_2, k_1, k_2, k) &= \langle p_2 K_3 p_1 \rangle \\ &\quad \times \left\{ \frac{\langle k K_2 K_1 k \rangle}{4(k_1 \cdot k)(k_2 \cdot k)} \left( \langle \xi \eta' \rangle^* - \langle \xi' \eta \rangle \right) - \langle k \xi \rangle^* \langle k \eta' \rangle^* \left[ \frac{1}{2(k_1 \cdot k)} + \frac{1}{2(k_2 \cdot k)} \right] \right\},\end{aligned}$$

$$\begin{aligned}A_{+, \tau_1, \tau_2, +}^{V_{te}}(p_1, p_2, k_1, k_2, k) &= \frac{1}{\langle k p_1 \rangle \langle k p_2 \rangle} \left[ g_{Vt}^- \langle \eta' (P_2 - K) p_1 \rangle \left( 2m_t \langle p_1 \eta \rangle + \langle \xi K_3 p_1 \rangle \right) \right. \\ &\quad \left. + g_{Vt}^+ \langle p_1 \xi' \rangle \left( 2m_t \langle \xi (P_2 - K) p_1 \rangle + \langle p_1 (P_2 - K) K_3 \eta \rangle^* \right) \right],\end{aligned}$$

$$\begin{aligned}A_{+, \tau_1, \tau_2, +}^{V_{tt}}(p_1, p_2, k_1, k_2, k) &= \\ &= \frac{1}{2(k_1 \cdot k)} P_t(k_1 + k_3) \left[ \langle k K_3 K_1 k \rangle P_t(k_1 + k_3 + k) - \frac{\langle k K_2 K_1 k \rangle}{2(k_2 \cdot k)} \right] \\ &\quad \times \left[ g_{Vt}^+ \langle p_1 \xi' \rangle \left( 2m_t \langle p_2 \xi \rangle^* - \langle p_2 K_3 \eta \rangle \right) + g_{Vt}^- \langle p_2 \eta' \rangle^* \left( 2m_t \langle p_1 \eta \rangle + \langle \xi K_3 p_1 \rangle \right) \right] \\ &\quad - \frac{\langle k \xi \rangle^*}{2(k_1 \cdot k)} P_t(k_1 + k_3 + k) \left[ 2g_{Vt}^+ m_t \langle p_1 \xi' \rangle \langle k p_2 \rangle^* - g_{Vt}^- \langle p_2 \eta' \rangle^* \langle k K_3 p_1 \rangle \right]\end{aligned}$$

$$\begin{aligned}
& + \frac{\langle k\eta' \rangle^* \langle kp_2 \rangle^*}{2(k_2 \cdot k)} P_t(k_1 + k_3) g_{V_t}^- [2m_t \langle p_1 \eta \rangle + \langle \xi K_3 p_1 \rangle] \\
& - \langle kp_2 \rangle^* \langle p_1 \xi' \rangle P_t(k_1 + k_3) P_t(k_1 + k_3 + k) g_{V_t}^+ [2m_t \langle k \xi \rangle^* - \langle k K_3 \eta \rangle], \\
A_{+, \tau_1, \tau_2, +}^{V\bar{t}e}(p_1, p_2, k_1, k_2, k) & = \frac{1}{\langle kp_1 \rangle \langle kp_2 \rangle} \left[ g_{V_t}^+ \langle \xi (P_2 - K) p_1 \rangle (2m_t \langle p_1 \xi' \rangle + \langle \eta' K_3 p_1 \rangle) \right. \\
& \left. + g_{V_t}^- \langle p_1 \eta \rangle (2m_t \langle \eta' (P_2 - K) p_1 \rangle + \langle p_1 (P_2 - K) K_3 \xi' \rangle^*) \right], \\
A_{+, \tau_1, \tau_2, +}^{V\bar{t}t}(p_1, p_2, k_1, k_2, k) & = \\
& = - \frac{1}{2(k_2 \cdot k)} P_t(k_2 + k_3) \left[ \langle k K_3 K_2 k \rangle P_t(k_2 + k_3 + k) + \frac{\langle k K_2 K_1 k \rangle}{2(k_1 \cdot k)} \right] \\
& \times \left[ g_{V_t}^+ \langle p_2 \xi \rangle^* (2m_t \langle p_1 \xi' \rangle + \langle \eta' K_3 p_1 \rangle) + g_{V_t}^- \langle p_1 \eta \rangle (2m_t \langle p_2 \eta' \rangle^* - \langle p_2 K_3 \xi' \rangle) \right] \\
& + \frac{\langle k\eta' \rangle^*}{2(k_2 \cdot k)} P_t(k_2 + k_3 + k) \left[ 2g_{V_t}^- m_t \langle p_1 \eta \rangle \langle kp_2 \rangle^* - g_{V_t}^+ \langle p_2 \xi \rangle^* \langle k K_3 p_1 \rangle \right] \\
& - \frac{\langle k\xi \rangle^* \langle kp_2 \rangle^*}{2(k_1 \cdot k)} P_t(k_2 + k_3) g_{V_t}^+ [2m_t \langle p_1 \xi' \rangle + \langle \eta' K_3 p_1 \rangle] \\
& + \langle kp_2 \rangle^* \langle p_1 \eta \rangle P_t(k_2 + k_3) P_t(k_2 + k_3 + k) g_{V_t}^- [2m_t \langle k\eta' \rangle^* - \langle k K_3 \xi' \rangle] \tag{2.35}
\end{aligned}$$

and the symmetry relations

$$\begin{aligned}
A_{-\sigma, \tau_1, \tau_2, \lambda}^{\dots t}(p_1, p_2, k_1, k_2, k) & = A_{\sigma \tau_1 \tau_2 \lambda}^{\dots t}(p_2, p_1, k_1, k_2, k), \\
A_{-\sigma, \tau_1, \tau_2, \lambda}^{\dots e}(p_1, p_2, k_1, k_2, k) & = -A_{\sigma \tau_1 \tau_2 \lambda}^{\dots e}(p_2, p_1, k_1, k_2, k), \\
A_{\sigma, -\tau_2, -\tau_1, -\lambda}^{Bf}(p_1, p_2, k_1, k_2, k) & = \text{sgn}(\tau_1 \tau_2) A_{\sigma \tau_1 \tau_2 \lambda}^{Bf}(p_2, p_1, k_2, k_1, k)^*, \quad B = Z, \chi, \quad f = e, t, \\
A_{\sigma, -\tau_2, -\tau_1, -\lambda}^{Vtf}(p_1, p_2, k_1, k_2, k) & = \text{sgn}(\tau_1 \tau_2) A_{\sigma \tau_1 \tau_2 \lambda}^{Vtf}(p_2, p_1, k_2, k_1, k)^*, \quad f = e, t, \\
A_{\sigma, -\tau_2, -\tau_1, -\lambda}^{V\bar{t}f}(p_1, p_2, k_1, k_2, k) & = \text{sgn}(\tau_1 \tau_2) A_{\sigma \tau_1 \tau_2 \lambda}^{V\bar{t}f}(p_2, p_1, k_2, k_1, k)^*, \quad f = e, t. \tag{2.36}
\end{aligned}$$

Note that interchanging  $k_1 \leftrightarrow k_2$  means also interchanging  $\eta \leftrightarrow \xi', \xi \leftrightarrow \eta'$ . Besides (2.19) we used the following auxiliary quantities in the previous definitions:

$$\begin{aligned}
\langle k K_2 K_1 k \rangle & = k_A K_2^{AB} K_{1, BC} k^{\dot{C}} = \sum_{i,j=1,2} \langle k \rho_i' \rangle^* \langle \rho_j \rho_i' \rangle \langle \rho_j k \rangle^*, \\
\langle k K_3 K_1 k \rangle & = k_A K_3^{AB} K_{1, BC} k^{\dot{C}} = \sum_{i,j=1,2} \langle k \phi_i \rangle^* \langle \rho_j \phi_i \rangle \langle \rho_j k \rangle^*, \\
\langle k K_3 K_2 k \rangle & = k_A K_3^{AB} K_{2, BC} k^{\dot{C}} = \sum_{i,j=1,2} \langle k \phi_i \rangle^* \langle \rho_j' \phi_i \rangle \langle \rho_j' k \rangle^*, \\
\langle \psi' (P_2 - K) K_3 \psi \rangle & = \psi_A' P_2^{AB} K_{3, BC} \psi^{\dot{C}} - \psi_A' K^{AB} K_{3, BC} \psi^{\dot{C}} \\
& = \sum_{j=1,2} (\langle \psi' p_2 \rangle^* \langle \phi_j p_2 \rangle \langle \phi_j \psi \rangle^* - \langle \psi' k \rangle^* \langle \phi_j k \rangle \langle \phi_j \psi \rangle^*). \tag{2.37}
\end{aligned}$$

The Weyl spinor  $k_A$  and the momentum matrix  $K_{AB}$  of the photon are defined from the photon momentum  $k$  analogously to those of the massless electron in (2.6) and (2.7).

The contribution  $\sigma_\gamma$  of the radiative process to the cross section is given by

$$\sigma_\gamma = \frac{1}{2s} \int d\Phi_\gamma \sum_{\sigma=\pm\frac{1}{2}} \frac{1}{4} (1 + 2P_{-\sigma})(1 - 2P_{+\sigma}) |\mathcal{M}_\gamma^\sigma|^2 \tag{2.38}$$

with

$$|\mathcal{M}_\gamma^\sigma|^2 = N_t^c \sum_{\lambda=\pm 1} \sum_{\tau_1=\pm\frac{1}{2}} \sum_{\tau_2=\pm\frac{1}{2}} |\mathcal{M}_\gamma^{\sigma\tau_1\tau_2\lambda}|^2, \quad (2.39)$$

and the phase-space integral

$$\int d\Phi_\gamma = \int \frac{d^3\mathbf{k}}{(2\pi)^3 2k^0} \left( \prod_{i=1}^3 \int \frac{d^3\mathbf{k}_i}{(2\pi)^3 2k_i^0} \right) (2\pi)^4 \delta\left(p_1 + p_2 - k - \sum_{j=1}^3 k_j\right). \quad (2.40)$$

The spin-averaged squared matrix element obtained from Eqs. (2.26)–(2.36) has been successfully checked against the result obtained with the package *Madgraph* [33] numerically.

### 2.3.2 Treatment of soft and collinear singularities

Without soft and collinear regulators the phase-space integral (2.38) diverges in the soft ( $k_0 \rightarrow 0$ ) and collinear ( $p_a k \rightarrow 0$ ) phase-space regions. In the following we describe two procedures of treating soft and collinear photon emission: one is based on a subtraction method, the other on phase-space slicing. In both cases soft and collinear singularities are regularized by an infinitesimal photon mass and a small electron mass, respectively.

Comparing both methods we find numerical agreement for total cross sections and distributions within integration errors. The results presented in this paper were obtained with the subtraction method, and the statistical error is typically 0.1% or below for the total cross section.

#### (i) The dipole subtraction approach

The idea of so-called subtraction methods is to subtract a simple auxiliary function from the singular integrand of the bremsstrahlung integral and to add this contribution back again after partial analytic integration. This auxiliary function, denoted  $|\mathcal{M}_{\text{sub}}|^2$  in the following, has to be chosen in such a way that it cancels all singularities of the original integrand, which is  $|\mathcal{M}_\gamma|^2$  in our case, so that the phase-space integration of the difference can be performed numerically, even over the singular regions of the original integrand. In this difference,  $\mathcal{M}_\gamma$  can be evaluated without regulators for soft or collinear singularities, i.e. we can make use of the results of the previous section. The auxiliary function has to be simple enough so that it can be integrated over the singular regions analytically, when the subtracted contribution is added again. This part contains the singular contributions and requires regulators, i.e. photon and electron masses have to be reintroduced there. Specifically, we have applied the *dipole subtraction formalism*, which is a process-independent approach that was first proposed [34] within QCD for massless unpolarized partons and subsequently generalized to photon radiation of massive polarized fermions in Ref. [35]. In order to keep the description of the method transparent, we describe only the basic structure of the individual terms explicitly and refer to Ref. [35] for details.

In the dipole subtraction formalism the subtraction functions are constructed from contributions related to ordered pairs of charged fermions. These two fermions are called

*emitter* and *spectator*, respectively, since by construction only the kinematics of the emitter leads to collinear singularities. In the following, we consider only the case for unpolarized final-state fermions. The subtraction function receives four kinds of contributions depending whether the emitter (first index) and spectator (second index) are chosen from initial (labelled by  $a, b$ ) or final state (denoted by  $i, j$ ):

$$|\mathcal{M}_{\text{sub}}^\sigma|^2 = \sum_{\substack{a,b=1,2 \\ a \neq b}} |\mathcal{M}_{\text{sub},ab}^\sigma|^2 + \sum_{\substack{a=1,2 \\ i=1,2}} \left( |\mathcal{M}_{\text{sub},ai}^\sigma|^2 + |\mathcal{M}_{\text{sub},ia}^\sigma|^2 \right) + \sum_{\substack{i,j=1,2 \\ i \neq j}} |\mathcal{M}_{\text{sub},ij}^\sigma|^2 \quad (2.41)$$

with the contributions

$$\begin{aligned} |\mathcal{M}_{\text{sub},ab}^\sigma|^2 &= e^2 g_{ab,+}^{(\text{sub})}(p_a, p_b, k) \left| \mathcal{M}_0^\sigma(\tilde{p}_1, \tilde{p}_2, \tilde{k}_1, \tilde{k}_2, \tilde{k}_3) \right|^2, \\ |\mathcal{M}_{\text{sub},ai}^\sigma|^2 &= (-1)^{a+i+1} Q_t e^2 g_{ai,+}^{(\text{sub})}(p_a, k_i, k) \left| \mathcal{M}_0^\sigma(\tilde{p}_1, \tilde{p}_2, \tilde{k}_1, \tilde{k}_2, \tilde{k}_3) \right|^2, \\ |\mathcal{M}_{\text{sub},ia}^\sigma|^2 &= (-1)^{a+i+1} Q_t e^2 g_{ia}^{(\text{sub})}(k_i, p_a, k) \left| \mathcal{M}_0^\sigma(\tilde{p}_1, \tilde{p}_2, \tilde{k}_1, \tilde{k}_2, \tilde{k}_3) \right|^2, \\ |\mathcal{M}_{\text{sub},ij}^\sigma|^2 &= Q_t^2 e^2 g_{ij}^{(\text{sub})}(k_i, k_j, k) \left| \mathcal{M}_0^\sigma(\tilde{p}_1, \tilde{p}_2, \tilde{k}_1, \tilde{k}_2, \tilde{k}_3) \right|^2. \end{aligned} \quad (2.42)$$

The unpolarized dipole functions for final-state emitters read

$$\begin{aligned} g_{ia}^{(\text{sub})}(k_i, p_a, k) &= g_{ia,+}^{(\text{sub})}(k_i, p_a, k) + g_{ia,-}^{(\text{sub})}(k_i, p_a, k), \\ g_{ij}^{(\text{sub})}(k_i, k_j, k) &= g_{ij,+}^{(\text{sub})}(k_i, k_j, k) + g_{ij,-}^{(\text{sub})}(k_i, k_j, k). \end{aligned} \quad (2.43)$$

The dipole functions  $g_{\dots}^{(\text{sub})}$  are defined in Eqs. (3.22), (A.1), and (4.4) of Ref. [35]. Note that the spin-flip dipole functions  $g_{ab,-}^{(\text{sub})}$  and  $g_{ai,-}^{(\text{sub})}$  vanish in the case of small fermion masses, i.e.  $m_e \rightarrow 0$ . The arguments  $\tilde{p}_a, \tilde{k}_i$  of the tree-level matrix elements  $\mathcal{M}_0^\sigma$  in subtraction functions depend on the momenta  $p_a, k_i, k$ . The mapping from  $p_a, k_i, k$  into  $\tilde{p}_a, \tilde{k}_i$  is defined by Eqs. (3.25) and (3.26) of Ref. [35] for  $\mathcal{M}_{\text{sub},ab}^\sigma$ , by Eq. (3.12) for  $\mathcal{M}_{\text{sub},ai}^\sigma$  and  $\mathcal{M}_{\text{sub},ia}^\sigma$ , and by Eq. (4.5) for  $\mathcal{M}_{\text{sub},ij}^\sigma$ .

The subtracted contribution can be integrated over the (singular) photonic degrees of freedom up to a remaining convolution over  $x$  ( $= x_{ab}, x_{ia}$ ). In this integration the regulators  $m_\gamma$  and  $m_e$  must be retained, and the soft and collinear singularities appear as logarithms in these mass regulators. This non-trivial step has, however, to be done only once and for all, and the needed results can be found in Ref. [35]. The integrated subtraction function reads

$$\begin{aligned} \sigma_{\text{sub}}(p_1, p_2, P_-, P_+) &= \\ &= \frac{\alpha}{2\pi} \int_0^1 dx \left\{ \sum_{\tau=\pm} \sum_{a=1,2} \int d\sigma_0^{(a,\tau)}(x) \left[ \sum_{\substack{b=1,2 \\ b \neq a}} \mathcal{G}_{ab,\tau}^{(\text{sub})}(s, x) + \sum_{i=1,2} (-1)^{a+i+1} Q_t \mathcal{G}_{ai,\tau}^{(\text{sub})}(t_{ai}, x) \right]_+ \right. \\ &\quad \left. + \sum_{\substack{a=1,2 \\ i=1,2}} \int d\sigma_0^{(a,+)}(x) (-1)^{a+i+1} Q_t \left[ \mathcal{G}_{ia}^{(\text{sub})}(t_{ai}, x) \right]_+ \right\} \\ &\quad + \frac{\alpha}{2\pi} \left\{ \sum_{\tau=\pm} \sum_{a=1,2} \int d\sigma_0^{(a,\tau)}(1) \left[ \sum_{\substack{b=1,2 \\ b \neq a}} G_{ab,\tau}^{(\text{sub})}(s) + \sum_{i=1,2} (-1)^{a+i+1} Q_t G_{ai,\tau}^{(\text{sub})}(t_{ai}) \right] \right. \\ &\quad \left. + \int d\sigma_0 \left[ \sum_{\substack{a=1,2 \\ i=1,2}} (-1)^{a+i+1} Q_t G_{ia}^{(\text{sub})}(t_{ai}) + \sum_{\substack{i,j=1,2 \\ i \neq j}} Q_t^2 G_{ij}^{(\text{sub})}(s_{ij}) \right] \right\} \end{aligned} \quad (2.44)$$

with the modified lowest-order cross sections

$$d\sigma_0^{(1,\tau)}(x) = d\sigma_0(xp_1, p_2, \tau P_-, P_+), \quad d\sigma_0^{(2,\tau)}(x) = d\sigma_0(p_1, xp_2, P_-, \tau P_+) \quad (2.45)$$

and the unpolarized distributions  $\mathcal{G}^{(\text{sub})}$  and end-point contributions  $G^{(\text{sub})}$ ,

$$\begin{aligned} \mathcal{G}_{ia}^{(\text{sub})}(t_{ai}, x) &= \mathcal{G}_{ia,+}^{(\text{sub})}(t_{ai}, x) + \mathcal{G}_{ia,-}^{(\text{sub})}(t_{ai}, x), \\ G_{ia}^{(\text{sub})}(t_{ai}) &= G_{ia,+}^{(\text{sub})}(t_{ai}) + G_{ia,-}^{(\text{sub})}(t_{ai}), \\ G_{ij}^{(\text{sub})}(s_{ij}) &= G_{ij,+}^{(\text{sub})}(s_{ij}) + G_{ij,-}^{(\text{sub})}(s_{ij}). \end{aligned} \quad (2.46)$$

In our case, the relevant definitions for  $\mathcal{G}^{(\text{sub})}$  and  $G^{(\text{sub})}$  are given in Eqs. (3.32), (3.33), (A.2), (A.4), and (4.10) of Ref. [35]. The  $[\dots]_+$  prescription is defined as usual,

$$\int_0^1 dx [f(x)]_+ g(x) \equiv \int_0^1 dx f(x) [g(x) - g(1)]. \quad (2.47)$$

In summary, the phase-space integral (2.38) in the dipole subtraction approach reads

$$\sigma_\gamma = \frac{1}{2s} \int d\Phi_\gamma \sum_{\sigma=\pm\frac{1}{2}} \frac{1}{4} (1 + 2P_- \sigma)(1 - 2P_+ \sigma) [|\mathcal{M}_\gamma^\sigma|^2 - |\mathcal{M}_{\text{sub}}^\sigma|^2] + \sigma_{\text{sub}}. \quad (2.48)$$

(ii) *The phase-space-slicing approach*

The idea of the phase-space-slicing method is to divide the bremsstrahlung phase space into singular and non-singular regions, then to evaluate the singular regions analytically and to perform an explicit cancellation of the arising soft and collinear singularities against their counterparts in the virtual corrections. The finite remainder can be evaluated by Monte Carlo techniques. For the actual implementation of this well-known procedure we closely follow the approach of Ref. [36]. We divide the four-particle phase space into soft and collinear regions by introducing the cut-off parameters  $\Delta E$  and  $\Delta\theta$ , respectively, and decompose the real corrections as

$$d\sigma_\gamma = d\sigma_{\text{soft}} + d\sigma_{\text{coll}} + d\sigma_{\gamma,\text{finite}}. \quad (2.49)$$

Here  $d\sigma_{\text{soft}}$  describes the contribution of the soft photons, i.e. of photons with energies  $k_0 < \Delta E$  in the CM frame, and  $d\sigma_{\text{coll}}$  describes real photon radiation outside the soft-photon region ( $k_0 > \Delta E$ ) but collinear to the  $e^\pm$  beams. The collinear region consists of the two disjoint parts  $0 < \theta_\gamma < \Delta\theta$  and  $\pi - \Delta\theta < \theta_\gamma < \pi$ , where  $\theta_\gamma$  is the polar angle of the emitted photon in the CM frame. The remaining part, which is free of singularities, is denoted by  $d\sigma_{\gamma,\text{finite}}$ .

In the soft and collinear regions, the squared matrix element  $|\mathcal{M}_\gamma^\sigma|^2$  factorizes into the leading-order squared matrix element  $|\mathcal{M}_0^\sigma|^2$  and a soft or collinear factor. Also the four-particle phase space factorizes into a three-particle phase space and a soft or collinear part, so that the integration over the singular part of the photon phase space can be performed analytically.

In the soft-photon region, we apply the soft-photon approximation to  $|\mathcal{M}_\gamma^\sigma|^2$ , i.e. the photon four-momentum  $k$  is omitted everywhere but in the IR-singular propagators. In this region  $d\sigma_\gamma$  can be written as [21, 37]

$$d\sigma_{\text{soft}} = -d\sigma_0 \frac{\alpha}{4\pi^2} \int_{\substack{k_0 < \Delta E \\ k_0^2 = |\mathbf{k}|^2 + m_\gamma^2}} \frac{d^3\mathbf{k}}{k_0} \left( \frac{p_1^\mu}{p_1 k} - \frac{p_2^\mu}{p_2 k} + Q_t \frac{k_1^\mu}{k_1 k} - Q_t \frac{k_2^\mu}{k_2 k} \right)^2. \quad (2.50)$$

This can be decomposed into an ISR part, a final-state-radiation (FSR) part (proportional to  $Q_t^2$ ) and the ISR–FSR-interference part (proportional to  $Q_t$ ),

$$d\sigma_{\text{soft}} = d\sigma_{\text{soft,ISR}} + d\sigma_{\text{soft,FSR}} + d\sigma_{\text{soft,int}}. \quad (2.51)$$

The explicit expressions for the soft-photon integrals can be found in Refs. [ 21, 28]. For our purpose it is sufficient to keep the electron mass only as regulator for the collinear singularities. In this limit we obtain for the ISR part

$$d\sigma_{\text{soft,ISR}} = -d\sigma_0 \frac{\alpha}{\pi} \left\{ 2 \ln \left( \frac{2\Delta E}{m_\gamma} \right) \left[ 1 - \ln \left( \frac{s}{m_e^2} \right) \right] - \ln \left( \frac{s}{m_e^2} \right) + \frac{1}{2} \ln^2 \left( \frac{s}{m_e^2} \right) + \frac{\pi^2}{3} \right\}. \quad (2.52)$$

The FSR part reads

$$d\sigma_{\text{soft,FSR}} = -d\sigma_0 \frac{\alpha}{4\pi^2} Q_t^2 [I_{tt} + I_{\bar{t}\bar{t}} - 2I_{t\bar{t}}] \quad (2.53)$$

with the massive integrals  $I_{ii}$  and  $I_{ij}$  from Refs. [ 21, 28]. Finally, the interference contribution is given by

$$d\sigma_{\text{soft,int}} = -d\sigma_0 \frac{\alpha}{2\pi^2} Q_t [I_{e^-t} - I_{e^- \bar{t}} - I_{e^+t} + I_{e^+ \bar{t}}] \quad (2.54)$$

in terms of the soft integral with a light particle  $a$  and a massive particle  $j$ ,

$$I_{aj} = 2\pi \left[ \ln \left( \frac{2\Delta E}{m_\gamma} \right) \ln \left( \frac{(2p_a p_j)^2}{m_a^2 m_j^2} \right) - \frac{1}{4} \ln^2 \left( \frac{m_j^2}{(p_j^0 + |\mathbf{p}_j|)^2} \right) - \frac{1}{4} \ln^2 \left( \frac{m_a^2}{(2p_a^0)^2} \right) - \frac{\pi^2}{6} \right. \\ \left. - \text{Li}_2 \left( 1 - \frac{p_a^0 m_j^2}{(p_j^0 + |\mathbf{p}_j|) p_a p_j} \right) - \text{Li}_2 \left( 1 - \frac{p_a^0 (p_j^0 + |\mathbf{p}_j|)}{p_a p_j} \right) \right]. \quad (2.55)$$

In the collinear region, we consider an incoming  $e^\mp$  with momentum  $p_a$  being split into a collinear photon and an  $e^\mp$  with the resulting momentum  $xp_a$  after photon radiation. The cross section for hard photon radiation ( $k_0 > \Delta E$ ) in this region reads

$$\sigma_{\text{coll}}(p_1, p_2, P_-, P_+) = \frac{\alpha}{2\pi} \int_0^{1-2\Delta E/\sqrt{s}} dx \sum_{\tau=\pm} \mathcal{G}_\tau^{(\text{coll})}(s, x) \left[ \int d\sigma_0^{(1,\tau)}(x) + \int d\sigma_0^{(2,\tau)}(x) \right], \quad (2.56)$$

where (2.45) is used, and

$$\mathcal{G}_+^{(\text{coll})}(s, x) = \frac{1+x^2}{1-x} \left[ \ln \left( \frac{s\Delta\theta^2}{4m_e^2} \right) - 1 \right], \quad \mathcal{G}_-^{(\text{coll})}(s, x) = 1 - x. \quad (2.57)$$

Finally, the finite cross section  $d\sigma_{\gamma,\text{finite}}$  is defined by imposing cuts on the bremsstrahlung phase space (2.40), i.e. a photon-energy cut,  $k_0 > \Delta E$ , and a cut on the angles  $\Delta\theta < \theta_\gamma < \pi - \Delta\theta$ .

For the numerical evaluation the values  $\Delta E/\sqrt{s} = 10^{-6}$  and  $\Delta\theta = 10^{-3}$  have been chosen. For  $\sqrt{s} = 500$  GeV and  $M_H = 140$  GeV as well as for  $\sqrt{s} = 1$  TeV and  $M_H = 115$  GeV, we have checked that the cross section changes only within integration errors when varying  $\Delta E$  within  $10^{-5}$  GeV  $< \Delta E < 10^{-2}$  GeV for fixed  $\Delta\theta = 10^{-3}$  and when varying  $\Delta\theta$  within  $10^{-5} < \Delta\theta < 10^{-2}$  for fixed  $\Delta E = 10^{-3}$  GeV.

## 2.4 QCD corrections

The  $\mathcal{O}(\alpha_s)$  QCD corrections can be obtained from the photonic FSR part of the  $\mathcal{O}(\alpha)$  correction, i.e. the part proportional to  $Q_t^2$ , by the replacement

$$Q_t^2 \alpha \rightarrow C_F \alpha_s(\mu^2) = \frac{4}{3} \alpha_s(\mu^2), \quad (2.58)$$

where  $Q_t = 2/3$  is the relative charge of the top quark. The real part of the FSR corrections results from diagrams where a photon is emitted from top quarks. The corresponding matrix elements  $\mathcal{M}_{\gamma}^{i \rightarrow t}$  are given in Eqs. (2.28), (2.30), (2.32), and (2.34). Following Ref. [12], the QCD renormalization scale  $\mu$  is set to the CM energy  $\sqrt{s}$ , and the running of the strong coupling is evaluated at the two-loop level ( $\overline{\text{MS}}$  scheme) with five active flavours, normalized by  $\alpha_s(M_Z^2)$  as given in (3.1). For  $\sqrt{s} = 500$  GeV, 800 GeV, and 1000 GeV the resulting values for the strong coupling are given by  $\alpha_s(M_Z^2) = 0.09349$ , 0.08857, and 0.08642, respectively.

## 2.5 Initial-state radiation beyond $\mathcal{O}(\alpha)$

The emission of photons collinear to the incoming electrons or positrons leads to corrections that are enhanced by large logarithms of the form  $\ln(m_e^2/s)$ . In order to achieve an accuracy at the few 0.1% level, the corresponding higher-order contributions, i.e. contributions beyond  $\mathcal{O}(\alpha)$ , must be taken into account. These are included in our calculation through a convolution of the leading-order cross section with leading-logarithmic structure functions precisely in the same way as described in Ref. [23].

## 2.6 Monte Carlo integration

The phase-space integration is performed with Monte Carlo techniques in both computer codes. The first code employs a multi-channel Monte Carlo generator similar to the one implemented in *RacoonWW* [38, 39] and *Lusifer* [40], the second one uses the adaptive multi-dimensional integration program *VEGAS* [41].

## 3 Numerical results

### 3.1 Input parameters

For the numerical evaluation we use the following set of SM parameters [42]:

$$\begin{aligned} G_\mu &= 1.16639 \times 10^{-5} \text{ GeV}^{-2}, & \alpha(0) &= 1/137.03599976, & \alpha_s(M_Z) &= 0.1172, \\ M_W &= 80.423 \text{ GeV}, & M_Z &= 91.1876 \text{ GeV}, \\ m_e &= 0.510998902 \text{ MeV}, & m_\mu &= 105.658357 \text{ MeV}, & m_\tau &= 1.77699 \text{ GeV}, \\ m_u &= 66 \text{ MeV}, & m_c &= 1.2 \text{ GeV}, & m_t &= 174.3 \text{ GeV}, \\ m_d &= 66 \text{ MeV}, & m_s &= 150 \text{ MeV}, & m_b &= 4.3 \text{ GeV}, \end{aligned} \quad (3.1)$$

which coincides with the one used in Refs. [20, 23]. Since we employ the on-shell renormalization scheme, the weak mixing angle is fixed by (2.4). Because quark mixing is irrelevant for the considered process we use a unit quark-mixing matrix.

We evaluate amplitudes in the so-called  $G_\mu$ -scheme, i.e. we derive the electromagnetic coupling  $\alpha = e^2/(4\pi)$  from the Fermi constant  $G_\mu$  according to

$$\alpha_{G_\mu} = \frac{\sqrt{2}G_\mu M_W^2 s_w^2}{\pi}. \quad (3.2)$$

This procedure, in particular, absorbs all sizable mass effects of light fermions other than electrons in the coupling  $\alpha_{G_\mu}$ , and the results are practically independent of the masses of the light quarks. The masses of the light quarks are adjusted to reproduce the hadronic contribution to the photonic vacuum polarization of Ref. [43]. In the relative radiative corrections, we use  $\alpha(0)$  as coupling parameter, which is the correct effective coupling for real photon emission. We do not calculate the W-boson mass from  $G_\mu$  but use its experimental value as input.

### 3.2 Results on total cross sections

Numerical results for total cross sections including individual contributions to the radiative corrections have already been presented in Ref. [20]. The contributions discussed there were the *photonic* corrections originating from virtual photon exchange and real photon radiation, the beyond  $\mathcal{O}(\alpha)$  or *higher-order ISR* corrections that are included using the structure-function approach as described above, and the remaining non-photonic *weak* corrections. All these have been combined into the complete *electroweak* corrections. Furthermore, the *QCD* corrections have been considered.

Here, we complement this by a splitting of the *weak* corrections into the purely *fermionic* loops together with the fermionic part of the counterterms and the remaining *weak bosonic* contributions. Instead of the separate *photonic* and *higher-order ISR* contributions considered in Ref. [20], we only look at their sum, denoted by *QED*. The corresponding relative corrections are shown as a function of the CM energy in Figure 13 for Higgs-boson masses of  $M_H = 115$  GeV and 150 GeV.

The fermionic corrections are about +10% and depend only weakly on the CM energy. While the weak bosonic contribution is also around +10% close to threshold, it falls off rapidly with increasing CM energies, eventually reaching about -20% at an energy of 1.5 TeV. Therefore, for energies above 600 GeV, the fermionic and weak bosonic contributions partially cancel when combined to form the complete weak corrections. The QED corrections are about -40% at threshold rising to a few per cent at 1.5 TeV. In the electroweak corrections, both QED and weak contributions partially compensate each other, yielding relative corrections of about -20% at threshold, and -3% and -7% for  $M_H = 115$  GeV and 150 GeV, respectively, at 1.5 TeV.

### 3.3 Results on distributions

The distributions in the Higgs-boson energy  $E_H$  and polar angle  $\theta_H$  are shown in Figure 14 for  $M_H = 115$  GeV and  $\sqrt{s} = 800$  GeV, where the cross section is nearly maximal for small Higgs-boson masses. All energies and angles used in the distributions here and below are defined in the CM frame. The curves denoted with *electroweak* contain only the electroweak corrections and (in case of the absolute distributions) the lowest-order contribution, whereas in the curve labelled *full* the QCD corrections are included as well.

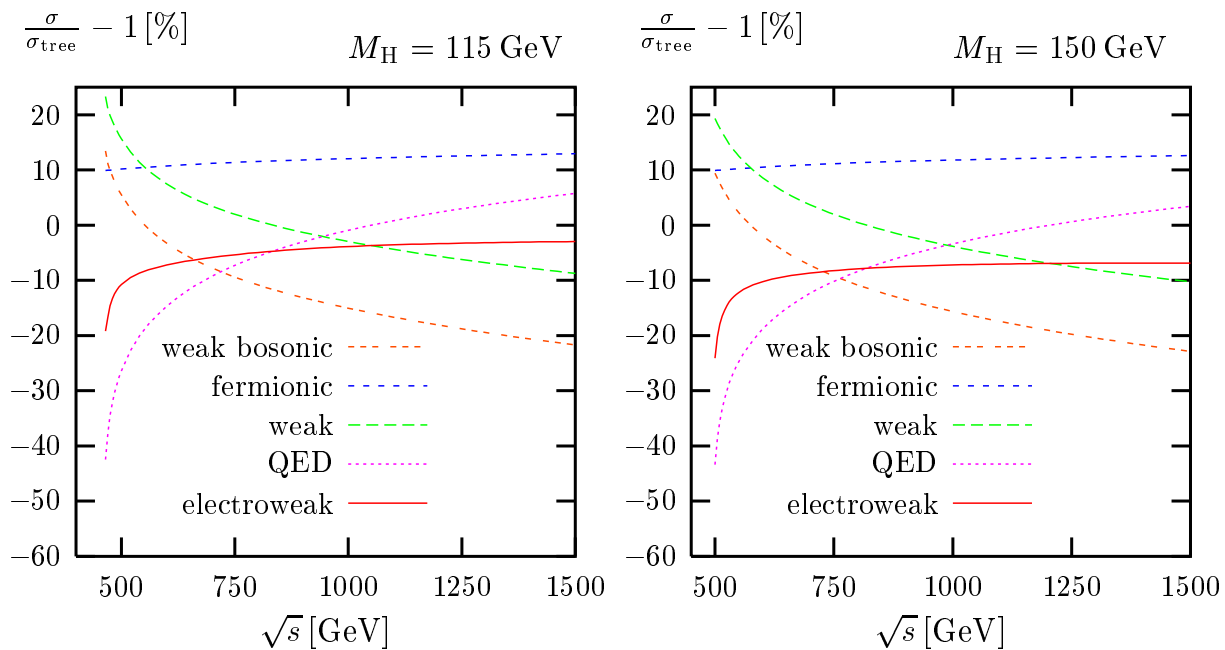


Figure 13: Relative corrections for  $M_H = 115$  GeV (l.h.s) and  $M_H = 150$  GeV (r.h.s)

The distribution in the Higgs-boson energy is a broad continuum whose maximum around 190 GeV gets slightly shifted down to smaller energies by the electroweak corrections but is left unchanged by the QCD corrections. At the upper end of the  $E_H$  spectrum the  $t\bar{t}$  system becomes non-relativistic, and the QCD correction is dominated by the Coulomb singularity [ 12, 14, 16] induced by soft-gluon exchange in the  $t\bar{t}$  system; the rising QCD correction with increasing  $E_H$  reflects the transition to this singular region. Although photonic FSR shows the same behaviour, this effect is totally overruled by ISR in the QED corrections. For increasing  $E_H$  these corrections become more and more negative because of the reduced phase space after ISR, which prohibits a cancellation of large IR-sensitive virtual corrections by the real corrections. For the chosen CM energy and Higgs-boson mass, the purely weak corrections depend only weakly on the Higgs-boson energy  $E_H$  and are only at the per-cent level. Note, however, that the smallness of the corrections for the chosen setup is mainly due to the transition from larger positive to negative corrections with increasing CM energy, as can be seen in Figure 13. Thus, for lower and higher CM energies sizeable weak corrections to the  $E_H$  spectrum arise.

The distribution in  $\cos\theta_H$  reaches maxima in the forward and backward directions at leading order. The inclusion of the radiative corrections does not sizeably distort this shape, and essentially only the normalization is changed. However, viewed separately the weak and photonic contributions show a small dependence on  $\theta_H$  which cancels in their sum.

Figure 15 shows the distributions in the top-quark energy  $E_t$  and in the cosine of the angle between the top quark and the incoming electron,  $\cos\theta_t$ , for  $\sqrt{s} = 800$  GeV and  $M_H = 115$  GeV. The  $E_t$  distribution has a broad peak at high energies, which is smeared out by the QED and QCD corrections towards lower energies. While the weak corrections vary only slowly with  $E_t$ , QCD and QED corrections decrease rapidly and reach large

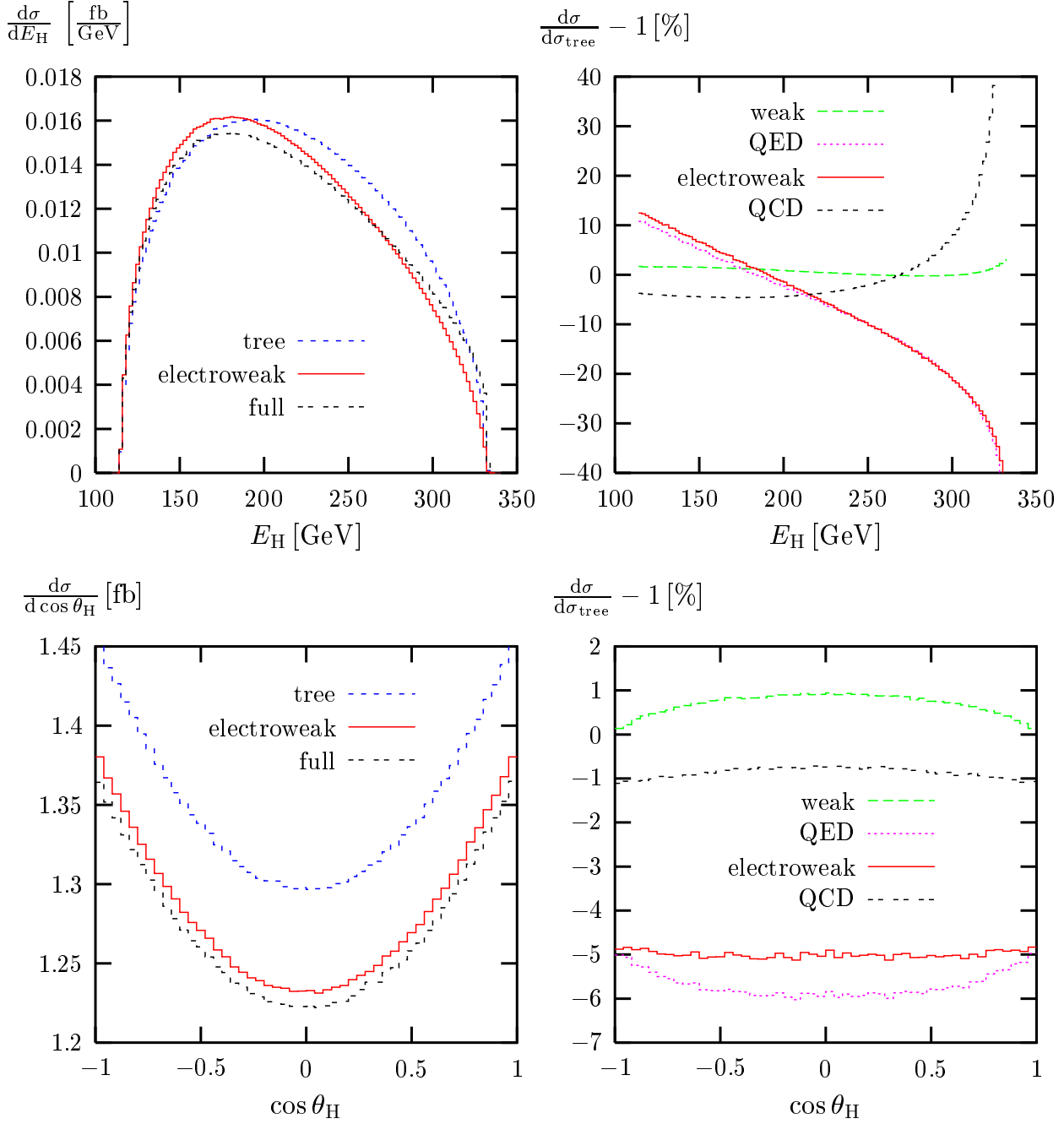


Figure 14: Distribution in the Higgs-boson energy  $E_H$  (upper panels) and the Higgs-boson polar angle  $\theta_H$  (lower panels) and corresponding relative corrections for  $\sqrt{s} = 800$  GeV and  $M_H = 115$  GeV

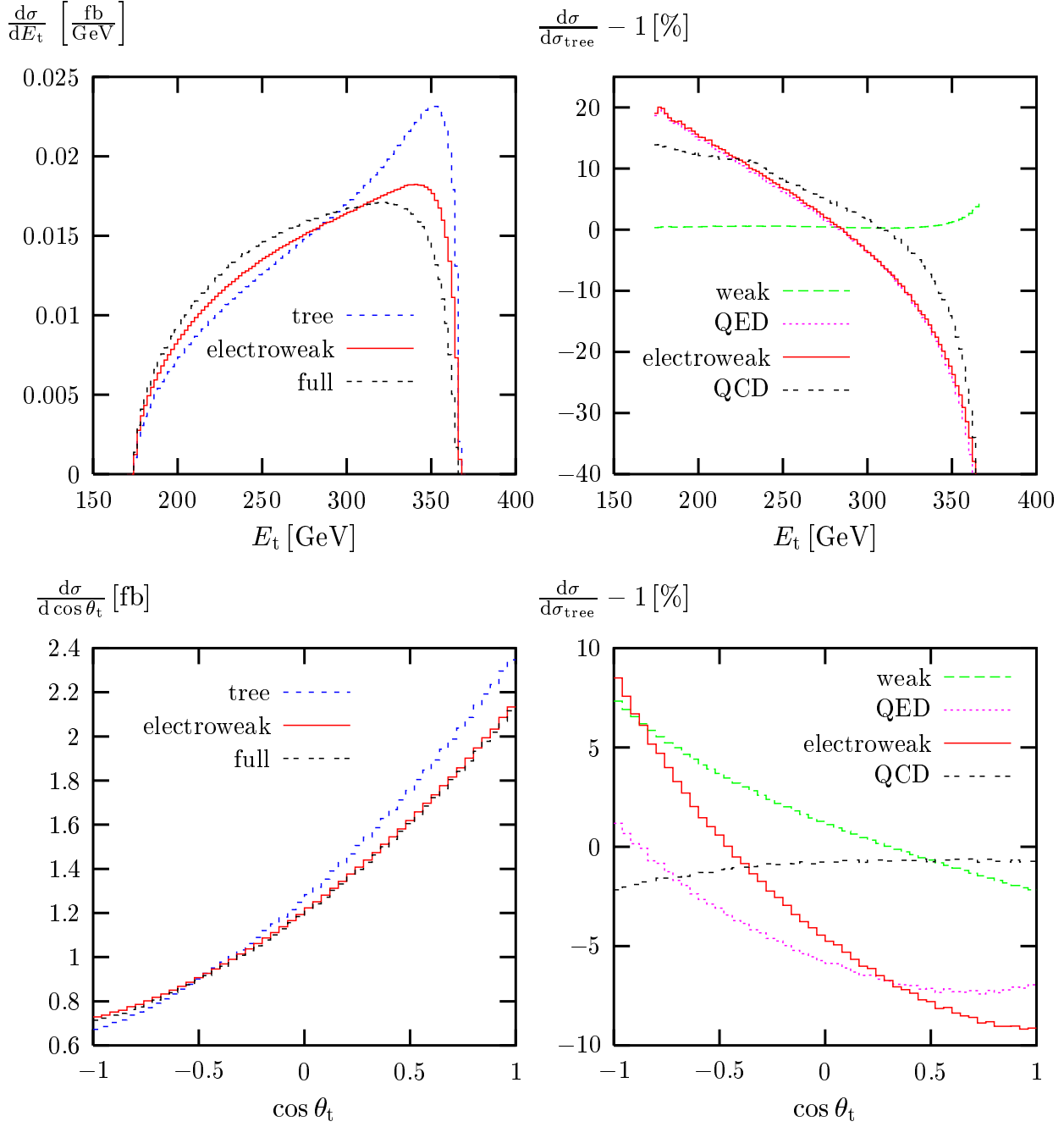


Figure 15: Distribution in the top-quark energy  $E_t$  (upper panels) and the top-quark polar angle  $\theta_t$  (lower panels) and corresponding relative corrections for  $\sqrt{s} = 800$  GeV and  $M_H = 115$  GeV

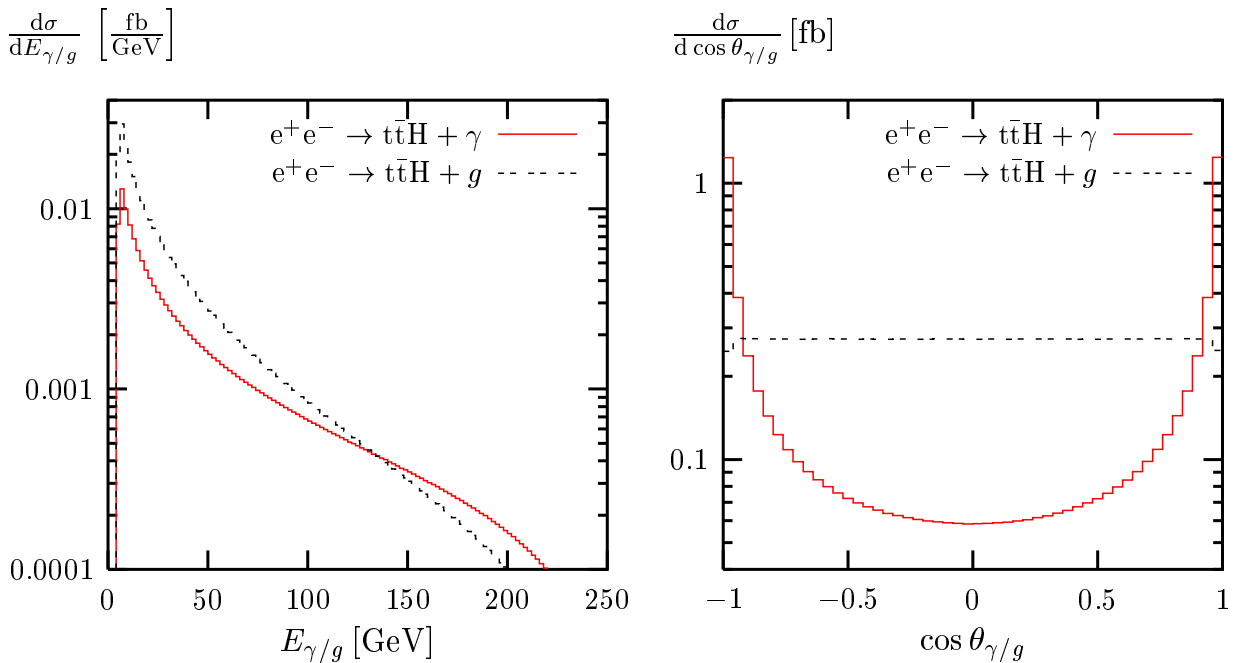


Figure 16: Distribution in the photon/gluon energy  $E_{\gamma/g}$  and in the photon/gluon polar angle  $\cos \theta_{\gamma/g}$  in the radiative processes  $e^+e^- \rightarrow t\bar{t}H + \gamma/g$  for  $\sqrt{s} = 800$  GeV and  $M_H = 115$  GeV

negative values for large  $E_t$ . This is due to the fact that for large  $E_t$ , the available phase space for the emission of a real photon or gluon is restricted and the large negative virtual corrections can only be partially compensated. The distribution in the top-quark production angle is maximal in the forward ( $e^-$ ) direction. The relative QCD corrections show only a small angular variation, but the weak and QED contributions, and hence the electroweak corrections, depend on  $\cos \theta_t$ , weakening the maximum somewhat. Owing to CP-symmetry the energy distribution of the anti-top quark is identical to the top-quark distribution. The angular distribution for the anti-top quark can be obtained from the one of the top quark by the replacement  $\cos \theta_t \rightarrow -\cos \theta_{\bar{t}}$ .

Finally, the spectra of the photon energy  $E_\gamma$  and of the photon polar angle  $\cos \theta_\gamma$  of the radiative process  $e^+e^- \rightarrow t\bar{t}H + \gamma$  are shown in Figure 16 together with the corresponding distributions for the gluon in the process  $e^+e^- \rightarrow t\bar{t}H + g$ , again for  $\sqrt{s} = 800$  GeV and  $M_H = 115$  GeV. In order to render the photon/gluon visible, we impose angular and energy cuts of

$$\theta(\gamma/g, \text{beam}) > 5^\circ, \quad E_{\gamma/g} > 5 \text{ GeV}. \quad (3.3)$$

The photon and gluon energy spectra are dominated by the IR pole in the region of small energies. Owing to the collinear singularity of ISR, the photon angular spectrum shows a strong peaking behaviour in the forward and backward directions. In contrast, for the chosen set-up the gluon radiation does not show a dependence on the gluon production angle. The reduction in the first and last bins is due to the angular cut.

## 4 Summary

If the Higgs boson is not too heavy, an experimental analysis of the process  $e^+e^- \rightarrow t\bar{t}H$  at a future high-energy  $e^+e^-$  linear collider allows for a determination of the top-quark–Higgs-boson coupling at the level of 5% or better. At this level of accuracy, the inclusion of both QCD and electroweak radiative corrections is important.

We have presented the calculation of the  $\mathcal{O}(\alpha)$  and  $\mathcal{O}(\alpha_s)$  radiative corrections to the process  $e^+e^- \rightarrow t\bar{t}H$  in the Standard Model in some detail. Particular attention has been paid to the treatment of the soft and collinear singularities in the real photonic (and gluonic) corrections.

Numerical results on the corrections to total cross sections are discussed, complementing existing work in the literature; in particular, the interplay of weak fermionic, weak bosonic, and photonic corrections is investigated. We find that all these contributions are typically at the level of 10% and that the different contributions partially cancel each other. Moreover, we have presented numerical results for the electroweak corrections to differential cross sections, including energy and angular distributions of the final-state particles. In the  $G_\mu$ -scheme the size of the corrections typically reaches the 10% level and even exceeds it near edges of phase space, underlining the importance of a thorough understanding of the radiative corrections.

## Appendix

### A Standard matrix elements

For the calculation of the loop corrections it is convenient to separate the matrix elements into scalar invariant coefficient functions containing the loop integrals and standard matrix elements (SME) containing all tensorial and spinorial objects and the dependence on the helicities of the external particles [ 21].

To introduce a compact notation for the SME, the tensors

$$\begin{aligned}\Gamma_{\{\mu,\mu\nu\rho\}}^{e^+e^-, \sigma} &= \bar{v}_{e^+}(p_2) \{ \gamma_\mu, \gamma_\mu \gamma_\nu \gamma_\rho \} \omega_\sigma u_{e^-}(p_1), \\ \Gamma_{\{1,\mu,\mu\nu,\dots\}}^{t\bar{t}, \tau} &= \bar{u}_t(k_1) \{ \mathbf{1}, \gamma_\mu, \gamma_\mu \gamma_\nu, \dots \} \omega_\tau v_{\bar{t}}(k_2)\end{aligned}\tag{A.1}$$

are defined with  $\omega_\pm = (1 \pm \gamma_5)/2$  and an obvious notation for the Dirac spinors  $u_{e^-}(p_1)$ , etc. Furthermore, symbols like  $\Gamma_p$  are used as shorthand for the contraction  $\Gamma_\mu p^\mu$ . In close analogy to the calculation [ 44] of QCD corrections to the related process  $q\bar{q} \rightarrow t\bar{t}H$ , we introduce the following set of SME,

$$\begin{aligned}\hat{\mathcal{M}}_{\{1,2,3,4\}}^{\sigma\tau} &= \Gamma^{e^+e^-, \sigma, \mu} \Gamma_{\{\mu, \mu p_1, \mu p_2, \mu p_1 p_2\}}^{t\bar{t}, \tau}, \\ \hat{\mathcal{M}}_{\{5,6,7,8\}}^{\sigma\tau} &= \Gamma^{e^+e^-, \sigma, \mu k_1 k_2} \Gamma_{\{\mu, \mu p_1, \mu p_2, \mu p_1 p_2\}}^{t\bar{t}, \tau}, \\ \hat{\mathcal{M}}_{\{9,10,11,12\}}^{\sigma\tau} &= \Gamma^{e^+e^-, \sigma, k_1} \Gamma_{\{1, p_1, p_2, p_1 p_2\}}^{t\bar{t}, \tau}, \\ \hat{\mathcal{M}}_{\{13,14,15,16\}}^{\sigma\tau} &= \Gamma^{e^+e^-, \sigma, k_2} \Gamma_{\{1, p_1, p_2, p_1 p_2\}}^{t\bar{t}, \tau}, \\ \hat{\mathcal{M}}_{\{17,18,19,20\}}^{\sigma\tau} &= \Gamma^{e^+e^-, \sigma, \mu\nu k_1} \Gamma_{\{\mu\nu, \mu\nu p_1, \mu\nu p_2, \mu\nu p_1 p_2\}}^{t\bar{t}, \tau},\end{aligned}$$

$$\begin{aligned}
\hat{\mathcal{M}}_{\{21,22,23,24\}}^{\sigma\tau} &= \Gamma^{e^+e^-, \sigma, \mu\nu k_2} \Gamma_{\{\mu\nu, \mu\nu p_1, \mu\nu p_2, \mu\nu p_1 p_2\}}^{\bar{t}\bar{t}, \tau}, \\
\hat{\mathcal{M}}_{\{25,26,27,28\}}^{\sigma\tau} &= \Gamma^{e^+e^-, \sigma, \mu\nu\rho} \Gamma_{\{\mu\nu\rho, \mu\nu\rho p_1, \mu\nu\rho p_2, \mu\nu\rho p_1 p_2\}}^{\bar{t}\bar{t}, \tau}.
\end{aligned} \tag{A.2}$$

The four-dimensionality of space–time implies that the SME  $\hat{\mathcal{M}}_i^{\sigma\tau}$  are not all independent; there are linear relations among them. A simple way to derive the relations with real coefficients is provided by the following trick. In four dimensions the metric tensor can be decomposed in terms of four independent orthonormal four-vectors  $n_l$ ,

$$g^{\alpha\beta} = n_0^\alpha n_0^\beta - \sum_{l=1}^3 n_l^\alpha n_l^\beta, \tag{A.3}$$

where  $n_k \cdot n_l = g_{kl}$ . Two convenient choices ( $j = 1, 2$ ) for the vectors  $n_l$  are given by

$$\begin{aligned}
n_0^\alpha &= \frac{1}{\sqrt{s}}(p_1 + p_2)^\alpha, & n_1^\alpha &= \frac{1}{\sqrt{s}}(p_1 - p_2)^\alpha, \\
n_2^\alpha &= \sqrt{\frac{s}{\bar{t}_{1j}\bar{t}_{2j} - m_t^2 s}} \left( k_j^\alpha + \frac{\bar{t}_{2j}}{s} p_1^\alpha + \frac{\bar{t}_{1j}}{s} p_2^\alpha \right), \\
n_3^\alpha &= \epsilon^{\alpha\beta\gamma\delta} n_{0,\beta} n_{1,\gamma} n_{2,\delta} = -\frac{2}{\sqrt{s(\bar{t}_{1j}\bar{t}_{2j} - m_t^2 s)}} \epsilon^{\alpha\beta\gamma\delta} p_{1,\beta} p_{2,\gamma} k_{j,\delta}
\end{aligned} \tag{A.4}$$

with

$$\bar{t}_{ij} = t_{ij} - m_t^2, \quad i, j = 1, 2, \tag{A.5}$$

and  $\epsilon^{\alpha\beta\gamma\delta}$  ( $\epsilon^{0123} = +1$ ) denoting the totally antisymmetric tensor. Inserting this decomposition for both  $j = 1, 2$  in all contractions between different Dirac chains according to  $\Gamma^{e^+e^-, \sigma, \alpha} \Gamma_\alpha^{\bar{t}\bar{t}, \tau} = \Gamma_\alpha^{e^+e^-, \sigma} g^{\alpha\beta} \Gamma_\beta^{\bar{t}\bar{t}, \tau}$ , etc., and subsequently using the Dirac equation and the Chisholm identity

$$i\epsilon^{\alpha\beta\gamma\delta} \gamma_\delta \gamma_5 = \gamma^\alpha \gamma^\beta \gamma^\gamma - g^{\alpha\beta} \gamma^\gamma + g^{\alpha\gamma} \gamma^\beta - g^{\beta\gamma} \gamma^\alpha \tag{A.6}$$

reduces all 112 SME  $\hat{\mathcal{M}}_i^{\sigma\tau}$  to 16. Further relations with complex coefficients result from the direct application of the Chisholm identity (A.6) to structures like  $\Gamma_{p_2 k_1 p_1}^{e^+e^-, \sigma}$  and subsequently using the decomposition

$$g^{\rho\sigma} = \sum_{i,j=1}^4 (Z^{-1})_{ij} 2p_i^\rho p_j^\sigma, \quad Z_{ij} = 2p_i p_j, \quad p_3 = k_1, \quad p_4 = k_2, \tag{A.7}$$

to separate all contractions between  $\epsilon$  tensors and Dirac chains via  $\Gamma_\delta^{e^+e^-, \sigma} \epsilon^{\alpha\beta\gamma\delta} = \Gamma_\rho^{e^+e^-, \sigma} g^{\rho\delta} \epsilon^{\alpha\beta\gamma}_\delta$ . For  $\Gamma_{p_2 k_1 p_1}^{e^+e^-, \pm}$ , in particular, this leads to

$$\Gamma_\delta^{e^+e^-, \sigma} \epsilon^{p_2 k_1 p_1 \delta} = \Gamma_\rho^{e^+e^-, \sigma} g^{\rho\delta} \epsilon^{p_2 k_1 p_1 \delta} = 2X \left[ \Gamma_{k_1}^{e^+e^-, \sigma} (Z^{-1})_{43} + \Gamma_{k_2}^{e^+e^-, \sigma} (Z^{-1})_{44} \right] \tag{A.8}$$

with

$$X = \epsilon^{p_1 p_2 k_1 k_2} = \epsilon^{\mu\nu\rho\sigma} p_{1,\mu} p_{2,\nu} k_{1,\rho} k_{2,\sigma}. \tag{A.9}$$

In the inverse matrix ( $Z^{-1}$ ), the determinant  $\det(Z)$  occurs, which can be identified with  $\det(Z) = -16X^2$ .

Altogether, the linear relations reduce the set of SME to 8 SME. It is convenient to express all SME in terms of  $\hat{\mathcal{M}}_1^{\sigma\tau}$ ,  $\hat{\mathcal{M}}_2^{\pm\pm}$ , and  $\hat{\mathcal{M}}_3^{\pm\mp}$  ( $\hat{\mathcal{M}}_2^{\pm\mp}$  and  $\hat{\mathcal{M}}_3^{\pm\pm}$  vanish),

$$\begin{aligned}
\hat{\mathcal{M}}_i^{++} &= a_i \hat{\mathcal{M}}_1^{++} + b_i \hat{\mathcal{M}}_1^{+-} + c_i \hat{\mathcal{M}}_2^{++} + d_i \hat{\mathcal{M}}_3^{+-}, \\
\hat{\mathcal{M}}_i^{--} &= a_i^* \hat{\mathcal{M}}_1^{--} + b_i^* \hat{\mathcal{M}}_1^{-+} + c_i^* \hat{\mathcal{M}}_2^{--} + d_i^* \hat{\mathcal{M}}_3^{-+}, \\
\hat{\mathcal{M}}_i^{+-} &= e_i \hat{\mathcal{M}}_1^{++} + f_i \hat{\mathcal{M}}_1^{+-} + g_i \hat{\mathcal{M}}_2^{++} + h_i \hat{\mathcal{M}}_3^{+-}, \\
\hat{\mathcal{M}}_i^{-+} &= e_i^* \hat{\mathcal{M}}_1^{--} + f_i^* \hat{\mathcal{M}}_1^{-+} + g_i^* \hat{\mathcal{M}}_2^{--} + h_i^* \hat{\mathcal{M}}_3^{-+}.
\end{aligned} \tag{A.10}$$

The non-vanishing coefficients  $a_i$ , etc., for the dependent SME read

$$\begin{aligned}
a_5 &= -\frac{D^* m_t^2 - 2\bar{s}_{12} \bar{t}_{12} \bar{t}_{22}}{2E_2}, & a_6 &= \frac{m_t (B^* \bar{t}_{11} - 2m_t^2 s \bar{t}_{12})}{2E_1}, \\
a_8 &= -\frac{\bar{t}_{22} (2m_t^2 s \bar{t}_{11} - C \bar{t}_{12})}{2E_2}, & a_9 &= \frac{m_t}{2}, & a_{10} &= -\frac{\bar{t}_{11}}{2}, \\
a_{11} &= \frac{A \bar{t}_{22}}{4E_2}, & a_{13} &= -\frac{A^* m_t}{4E_1}, & a_{14} &= \frac{A^* \bar{t}_{11}}{4E_1}, \\
a_{15} &= -\frac{\bar{t}_{22}}{2}, & a_{17} &= 2m_t, & a_{18} &= -4\bar{t}_{11}, \\
a_{19} &= \frac{2A \bar{t}_{22}}{E_2}, & a_{21} &= -\frac{A^* m_t}{E_1}, & a_{22} &= -4\bar{t}_{12}, \\
a_{23} &= -4\bar{t}_{22}, & a_{25} &= 16,
\end{aligned} \tag{A.11}$$

$$\begin{aligned}
b_9 &= \frac{A m_t}{4E_2}, & b_{12} &= \frac{A m_t s}{4E_2}, & b_{13} &= -\frac{m_t}{2}, \\
b_{16} &= -\frac{m_t s}{2}, & b_{17} &= \frac{A m_t}{E_2}, & b_{20} &= \frac{A m_t s}{E_2}, \\
b_{21} &= -2m_t, & b_{24} &= -2m_t s,
\end{aligned} \tag{A.12}$$

$$\begin{aligned}
c_6 &= -\frac{A^* m_t^2}{2E_1}, & c_9 &= \frac{2m_t^2 s \bar{t}_{21} - B \bar{t}_{22}}{4E_2 s}, & c_{10} &= \frac{m_t}{2}, \\
c_{12} &= -\frac{A \bar{t}_{22}}{4E_2}, & c_{13} &= \frac{C^* \bar{t}_{21} - 2m_t^2 s \bar{t}_{22}}{4E_1 s}, & c_{14} &= -\frac{A^* m_t}{4E_1}, \\
c_{16} &= \frac{\bar{t}_{22}}{2}, & c_{17} &= \frac{2m_t^2 s \bar{t}_{21} - B \bar{t}_{22}}{E_2 s}, & c_{20} &= -\frac{A \bar{t}_{22}}{E_2}, \\
c_{21} &= \frac{C^* \bar{t}_{21} - 2m_t^2 s \bar{t}_{22}}{E_1 s}, & c_{24} &= 2\bar{t}_{22}, & c_{26} &= 4,
\end{aligned} \tag{A.13}$$

$$\begin{aligned}
d_5 &= \frac{m_t (2m_t^2 s \bar{t}_{11} - C \bar{t}_{12})}{2E_2 s}, & d_8 &= \frac{m_t (2m_t^2 s \bar{t}_{11} - C \bar{t}_{12})}{2E_2}, & d_{11} &= -\frac{A m_t}{4E_2}, \\
d_{15} &= \frac{m_t}{2}, & d_{19} &= -\frac{2A m_t}{E_2}, & d_{23} &= 4m_t,
\end{aligned} \tag{A.14}$$

$$\begin{aligned}
e_6 &= -\frac{m_t(2m_t^2 s \bar{t}_{11} - C \bar{t}_{12})}{2E_2}, & e_9 &= \frac{Am_t}{4E_2}, & e_{13} &= -\frac{m_t}{2}, \\
e_{17} &= \frac{2Am_t}{E_2}, & e_{21} &= -4m_t, & & 
\end{aligned} \tag{A.15}$$

$$\begin{aligned}
f_4 &= s, & f_5 &= -\frac{A^* m_t^2}{2E_1}, & f_8 &= -\frac{A^* m_t^2 s}{2E_1}, \\
f_9 &= \frac{m_t}{2}, & f_{10} &= \frac{A \bar{t}_{12}}{4E_2}, & f_{11} &= -\frac{\bar{t}_{21}}{2}, \\
f_{12} &= \frac{m_t s}{2}, & f_{13} &= -\frac{A^* m_t}{4E_1}, & f_{14} &= -\frac{\bar{t}_{12}}{2}, \\
f_{15} &= \frac{A^* \bar{t}_{21}}{4E_1}, & f_{16} &= -\frac{A^* m_t s}{4E_1}, & f_{18} &= \frac{A \bar{t}_{12}}{E_2}, \\
f_{19} &= -2\bar{t}_{21}, & f_{22} &= -2\bar{t}_{12}, & f_{23} &= \frac{A^* \bar{t}_{21}}{E_1}, \\
f_{25} &= 4, & f_{28} &= 4s, & & 
\end{aligned} \tag{A.16}$$

$$\begin{aligned}
g_{10} &= -\frac{Am_t}{4E_2}, & g_{14} &= \frac{m_t}{2}, & g_{18} &= -\frac{Am_t}{E_2}, \\
g_{22} &= 2m_t, & & & & 
\end{aligned} \tag{A.17}$$

$$\begin{aligned}
h_5 &= \frac{m_t(B^* \bar{t}_{11} - 2m_t^2 s \bar{t}_{12})}{2E_1 s}, & h_6 &= \frac{\bar{t}_{12}(2m_t^2 s \bar{t}_{11} - C \bar{t}_{12})}{2E_2 s}, & h_7 &= \frac{B^*}{2s}, \\
h_8 &= \frac{m_t(B^* \bar{t}_{11} - 2m_t^2 s \bar{t}_{12})}{2E_1}, & h_9 &= \frac{2m_t^2 s \bar{t}_{11} - C \bar{t}_{12}}{4E_2 s}, & h_{11} &= \frac{m_t}{2}, \\
h_{12} &= -\frac{\bar{t}_{11}}{2}, & h_{13} &= \frac{B^* \bar{t}_{11} - 2m_t^2 s \bar{t}_{12}}{4E_1 s}, & h_{15} &= -\frac{A^* m_t}{4E_1}, \\
h_{16} &= \frac{A^* \bar{t}_{11}}{4E_1}, & h_{17} &= \frac{2(2m_t^2 s \bar{t}_{11} - C \bar{t}_{12})}{E_2 s}, & h_{19} &= 2m_t, \\
h_{20} &= -4\bar{t}_{11}, & h_{23} &= -\frac{A^* m_t}{E_1}, & h_{24} &= -4\bar{t}_{12}, \\
h_{27} &= 16, & & & & 
\end{aligned} \tag{A.18}$$

where the following shorthands are used,

$$\begin{aligned}
A &= s \bar{s}_{12} - \bar{t}_{12} \bar{t}_{21} - \bar{t}_{11} \bar{t}_{22} + 4iX, & B &= s \bar{s}_{12} + \bar{t}_{12} \bar{t}_{21} - \bar{t}_{11} \bar{t}_{22} + 4iX, \\
C &= s \bar{s}_{12} - \bar{t}_{12} \bar{t}_{21} + \bar{t}_{11} \bar{t}_{22} + 4iX, & D &= s \bar{s}_{12} + \bar{t}_{12} \bar{t}_{21} + \bar{t}_{11} \bar{t}_{22} + 4iX, \\
E_i &= -m_t^2 s + \bar{t}_{1i} \bar{t}_{2i}, & i &= 1, 2,
\end{aligned} \tag{A.19}$$

and

$$\bar{s}_{12} = s_{12} - 2m_t^2. \tag{A.20}$$

Finally, we give the explicit expressions of the independent SME  $\hat{\mathcal{M}}_1^{\sigma\tau}$ ,  $\hat{\mathcal{M}}_2^{\pm\pm}$ , and  $\hat{\mathcal{M}}_3^{\pm\mp}$  in terms of Weyl–van der Waerden spinor products as introduced in Section 2.1,

$$\begin{aligned}
\hat{\mathcal{M}}_1^{++} &= 2\langle p_2\xi\rangle^*\langle p_1\xi'\rangle, & \hat{\mathcal{M}}_1^{--} &= 2\langle p_1\eta'\rangle^*\langle p_2\eta\rangle, \\
\hat{\mathcal{M}}_1^{+-} &= 2\langle p_2\eta'\rangle^*\langle p_1\eta\rangle, & \hat{\mathcal{M}}_1^{-+} &= 2\langle p_1\xi\rangle^*\langle p_2\xi'\rangle, \\
\hat{\mathcal{M}}_2^{++} &= 2\langle p_1p_2\rangle^*\langle p_1\xi'\rangle\langle p_1\eta\rangle, & \hat{\mathcal{M}}_2^{--} &= -2\langle p_1\xi\rangle^*\langle p_1\eta'\rangle^*\langle p_1p_2\rangle, \\
\hat{\mathcal{M}}_3^{+-} &= 2\langle p_2\xi\rangle^*\langle p_2\eta'\rangle^*\langle p_1p_2\rangle, & \hat{\mathcal{M}}_3^{-+} &= -2\langle p_1p_2\rangle^*\langle p_2\xi'\rangle\langle p_2\eta\rangle,
\end{aligned} \tag{A.21}$$

where the insertions for the spinors  $\xi^{(l)}$  and  $\eta^{(l)}$  for the polarizations  $\tau_{1,2}$  are specified in Eq. (2.14).

## B Lowest-order and one-loop amplitudes in terms of standard matrix elements

Both lowest-order and one-loop amplitudes can be written as linear combination of the SME defined in Eq. (A.2). The contributions to the lowest-order amplitude  $\mathcal{M}_0$ , as defined in Eq. (2.16), take the simple form

$$\begin{aligned}
\mathcal{M}_0^{Z,\sigma} &= \sum_{\tau=\pm} e^3 \frac{g_{Ze}^\sigma g_{ZZH} g_{Zt}^\tau}{(s - M_Z^2)(s_{12} - M_Z^2)} \hat{\mathcal{M}}_1^{\sigma\tau}, \\
\mathcal{M}_0^{\chi,\sigma} &= \sum_{\tau=\pm} 2e^3 \frac{g_{Ze}^\sigma g_{Z\chi H} g_{\chi t}^\tau}{(s - M_Z^2)(s_{12} - M_Z^2)} (\hat{\mathcal{M}}_9^{\sigma\tau} + \hat{\mathcal{M}}_{13}^{\sigma\tau}), \\
\mathcal{M}_0^{Vt,\sigma} &= \sum_{\tau=\pm} e^3 \frac{g_{Ve}^\sigma g_{Vt}^\tau g_{Ht}}{(s - M_V^2)(s_{13} - m_t^2)} \\
&\quad \times [\hat{\mathcal{M}}_2^{\sigma\tau} + \hat{\mathcal{M}}_3^{\sigma\tau} + 2\hat{\mathcal{M}}_{13}^{\sigma\tau} - m_t(\hat{\mathcal{M}}_1^{\sigma\tau} - \hat{\mathcal{M}}_1^{\sigma,-\tau})], \\
\mathcal{M}_0^{V\bar{t},\sigma} &= \sum_{\tau=\pm} e^3 \frac{g_{Ve}^\sigma g_{V\bar{t}}^\tau g_{Ht}}{(s - M_V^2)(s_{23} - m_t^2)} \\
&\quad \times [\hat{\mathcal{M}}_2^{\sigma,-\tau} + \hat{\mathcal{M}}_3^{\sigma,-\tau} - 2\hat{\mathcal{M}}_9^{\sigma,-\tau} - m_t(\hat{\mathcal{M}}_1^{\sigma\tau} - \hat{\mathcal{M}}_1^{\sigma,-\tau})].
\end{aligned} \tag{B.1}$$

The one-loop amplitude  $\mathcal{M}_1^\sigma$  is much too lengthy to be written down; it is of the form

$$\mathcal{M}_1^\sigma = \sum_{i=1}^{28} \sum_{\tau=\pm} F_i^{\sigma\tau} \hat{\mathcal{M}}_i^{\sigma\tau}, \tag{B.2}$$

where the coefficient functions  $F_i^{\sigma\tau}$  depend on couplings and scalar products of external momenta and contain all loop integrals. Note that here  $\tau$  is related to the chirality projectors  $\omega_\tau$ , whereas in Section 2.1  $\tau_1, \tau_2$  denote the helicities of the external fermions.

## Acknowledgements

This work was supported in part by the Swiss Bundesamt für Bildung und Wissenschaft and by the European Union under contract HPRN-CT-2000-00149.

## References

- [1] The LEP Working Group for Higgs Boson Searches, LHWG Note/2002-01.
- [2] M. W. Grünewald, in the proceedings of the workshop on *Electroweak Precision Data and the Higgs Mass*, eds. S. Dittmaier and K. Mönig, (DESY-PROC-2003-50, Zeuthen, 2003), p. 1, hep-ex/0304023.
- [3] E. Accomando *et al.* [ECFA/DESY LC Physics Working Group Collaboration], Phys. Rept. **299** (1998) 1 [hep-ph/9705442];  
J. A. Aguilar-Saavedra *et al.*, TESLA Technical Design Report Part III: Physics at an  $e^+e^-$  Linear Collider [hep-ph/0106315];  
K. Abe *et al.* [ACFA Linear Collider Working Group Collaboration], ACFA Linear Collider Working Group report, [hep-ph/0109166];  
T. Abe *et al.* [American Linear Collider Working Group Collaboration], in *Proc. of the APS/DPF/DPB Summer Study on the Future of Particle Physics (Snowmass 2001)* ed. R. Davidson and C. Quigg, SLAC-R-570, *Resource book for Snowmass 2001* [hep-ex/0106055, hep-ex/0106056, hep-ex/0106057, hep-ex/0106058].
- [4] J. F. Gunion, B. Grzadkowski and X. G. He, Phys. Rev. Lett. **77** (1996) 5172 [hep-ph/9605326].
- [5] H. Baer, S. Dawson and L. Reina, Phys. Rev. D **61** (2000) 013002 [hep-ph/9906419];  
A. Juste and G. Merino, hep-ph/9910301.
- [6] M. Battaglia and K. Desch, hep-ph/0101165 and LC-PHSM-2001-053.
- [7] T. Han *et al.*, Phys. Rev. D **61** (2000) 015006 [hep-ph/9908236].
- [8] S. Moretti, Phys. Lett. B **452** (1999) 338 [hep-ph/9902214].
- [9] K. J. Gaemers and G. J. Gounaris, Phys. Lett. B **77** (1978) 379;  
A. Djouadi, J. Kalinowski and P. M. Zerwas, Mod. Phys. Lett. A **7** (1992) 1765 and  
Z. Phys. C **54** (1992) 255.
- [10] S. Dawson and L. Reina, Phys. Rev. D **57** (1998) 5851 [hep-ph/9712400].
- [11] S. Dawson and L. Reina, Phys. Rev. D **59** (1999) 054012 [hep-ph/9808443].
- [12] S. Dittmaier *et al.*, Phys. Lett. B **441** (1998) 383 [hep-ph/9808433].
- [13] S. Dawson and L. Reina, Phys. Rev. D **60** (1999) 015003 [hep-ph/9812488].
- [14] S. Dittmaier *et al.*, Phys. Lett. B **478** (2000) 247 [hep-ph/0002035].
- [15] S. Zhu, hep-ph/0212273.
- [16] S. Dittmaier, M. Krämer, M. Spira and P. M. Zerwas, LC-TH-2001-069.
- [17] Y. You *et al.*, Phys. Lett. B **571** (2003) 85 [hep-ph/0306036].

- [18] G. Bélanger *et al.*, hep-ph/0307029.
- [19] X. H. Wu, C. S. Li and J. J. Liu, hep-ph/0308012.
- [20] A. Denner, S. Dittmaier, M. Roth and M. M. Weber, hep-ph/0307193, to appear in Phys. Lett. B.
- [21] A. Denner, Fortsch. Phys. **41** (1993) 307.
- [22] S. Dittmaier, Phys. Rev. D **59** (1999) 016007 [hep-ph/9805445].
- [23] A. Denner, S. Dittmaier, M. Roth and M. M. Weber, Phys. Lett. B **560** (2003) 196 [hep-ph/0301189] and Nucl. Phys. B **660** (2003) 289 [hep-ph/0302198].
- [24] W. F. L. Hollik, Fortsch. Phys. **38** (1990) 165.
- [25] J. Küblbeck, M. Böhm and A. Denner, Comput. Phys. Commun. **60** (1990) 165; H. Eck and J. Küblbeck, *Guide to FeynArts 1.0*, University of Würzburg, 1992.
- [26] G. Passarino and M. Veltman, Nucl. Phys. B **160** (1979) 151.
- [27] A. Denner and S. Dittmaier, Nucl. Phys. B **658** (2003) 175 [hep-ph/0212259].
- [28] G. 't Hooft and M. Veltman, Nucl. Phys. B **153** (1979) 365; W. Beenakker and A. Denner, Nucl. Phys. B **338** (1990) 349.
- [29] S. Dittmaier, hep-ph/0308246.
- [30] T. Hahn, Comput. Phys. Commun. **140** (2001) 418 [hep-ph/0012260].
- [31] T. Hahn and M. Perez-Victoria, Comput. Phys. Commun. **118** (1999) 153 [hep-ph/9807565]; T. Hahn, Nucl. Phys. Proc. Suppl. **89** (2000) 231 [hep-ph/0005029].
- [32] A. Denner, S. Dittmaier and G. Weiglein, Nucl. Phys. B **440** (1995) 95 [hep-ph/9410338].
- [33] T. Stelzer and W. F. Long, Comput. Phys. Commun. **81** (1994) 357 [hep-ph/9401258]; H. Murayama, I. Watanabe and K. Hagiwara, KEK-91-11.
- [34] S. Catani and M. H. Seymour, Phys. Lett. B **378** (1996) 287 [hep-ph/9602277] and Nucl. Phys. B **485** (1997) 291 [Erratum-ibid. B **510** (1997) 291] [hep-ph/9605323].
- [35] S. Dittmaier, Nucl. Phys. B **565** (2000) 69 [hep-ph/9904440].
- [36] M. Böhm and S. Dittmaier, Nucl. Phys. B **409** (1993) 3 and B **412** (1994) 39.
- [37] D. R. Yennie, S. C. Frautschi and H. Suura, Annals Phys. **13** (1961) 379.
- [38] M. Roth, PhD thesis, ETH Zürich No. 13363 (1999), hep-ph/0008033.
- [39] A. Denner, S. Dittmaier, M. Roth and D. Wackerroth, Nucl. Phys. B **560** (1999) 33 [hep-ph/9904472].

- [40] S. Dittmaier and M. Roth, Nucl. Phys. B **642** (2002) 307 [hep-ph/0206070].
- [41] G. P. Lepage, J. Comput. Phys. **27** (1978) 192 and CLNS-80/447.
- [42] K. Hagiwara *et al.* [Particle Data Group Collaboration], Phys. Rev. D **66** (2002) 010001.
- [43] F. Jegerlehner, DESY 01-029, LC-TH-2001-035, hep-ph/0105283.
- [44] W. Beenakker *et al.*, Nucl. Phys. B **653** (2003) 151 [hep-ph/0211352].